



## SiO<sub>2</sub>/WO<sub>3</sub>/ZnO based self-cleaning coatings for solar cells

Ozcan Koysuren<sup>1</sup> · Klodian Dhoska<sup>2</sup> · Hafize Nagehan Koysuren<sup>3</sup> · Irida Markja<sup>2</sup> · Savas Yaglikci<sup>1</sup> · Bilge Tuncel<sup>1</sup> · Elena Bebi<sup>4</sup>

Received: 4 December 2023 / Accepted: 18 February 2024 / Published online: 6 March 2024  
© The Author(s) 2024

### Abstract

The accumulation of pollution and any kinds of contamination on the glass cover of the solar cell affects the efficiency of the photovoltaic (PV) systems. The contamination on the glass cover can absorb and reflect a certain part of the sunlight irradiation, which can decrease the intensity of the light coming in through the glass cover. With the study, it was planned to develop self-cleaning coatings for the PV systems. It was aimed to prevent or reduce the contamination-induced efficiency loss of the existing PV systems. In the scope of the project, SiO<sub>2</sub>/WO<sub>3</sub> and SiO<sub>2</sub>/WO<sub>3</sub>/ZnO composites were coated from their solutions on the glass substrates using a dip-coating technique. WO<sub>3</sub> was selected as a photocatalyst semiconductor. Under the UV light irradiation, WO<sub>3</sub> could absorb the photons of the UV light, generating the photoinduced charge carriers. The photoexcited charge carriers provide both the photoinduced hydrophilicity on the surface of the coating and the photocatalytic degradation of the organic contaminants accumulated on the surface of the coating, which allows water droplets to spread and flow on the surface of the cover glass to remove the contaminations. However, the recombination rate of the photoexcited charge carriers on the WO<sub>3</sub> film was high. In order to suppress the recombination of the photoinduced charge carriers, WO<sub>3</sub> was coupled with SiO<sub>2</sub> and ZnO. Both of these semiconductors improved the photocatalytic activity of the WO<sub>3</sub> film. Although SiO<sub>2</sub> has superior features in terms of the light transmission, it was not very effective under UV light as a photocatalyst alone. The widely preferred photocatalyst ZnO was added into the composite film structure to enhance the photocatalytic activity. The self-cleaning mechanism of the film coatings on a solar cell was investigated through the photocatalytic dye removal efficiency on the as-prepared film samples. There was a slight decrease in the light transparency and the solar cell efficiency because of the WO<sub>3</sub> content of the composite film. On the other hand, coupling the SiO<sub>2</sub>/WO<sub>3</sub> film with ZnO enhanced the photocatalytic activity, and it suppressed the reduction effect of the WO<sub>3</sub> phase on both the light transparency and the solar cell efficiency. The photocatalytic dye removal efficiency was increased to over 90% after 240 min of UVA light irradiation. In addition, the solar cell coated with the SiO<sub>2</sub>/WO<sub>3</sub>/ZnO film provided almost the same solar cell efficiency as the uncoated solar cell. The water contact angle measurement also exhibited the photocatalytic degradation of the model contamination on the glass cover of the solar cell under the UVA light irradiation.

✉ Ozcan Koysuren  
koysuren@ankara.edu.tr

✉ Klodian Dhoska  
kdhoska@fim.edu.al

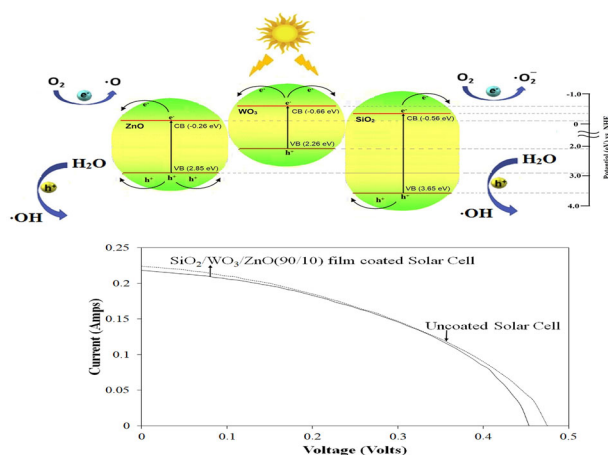
<sup>1</sup> Department of Energy Systems Engineering, Ankara University, Ankara 06830, Turkey

<sup>2</sup> Department of Production and Management, Faculty of Mechanical Engineering, Polytechnic University of Tirana, Tirana 1001, Albania

<sup>3</sup> Department of Environmental Engineering, Kirsehir Ahi Evran University, Kirsehir 40100, Turkey

<sup>4</sup> Energy Department, Faculty of Mechanical Engineering, Polytechnic University of Tirana, Tirana 1001, Albania

## Graphical Abstract



**Keywords** Self-cleaning coatings · Solar cell · Photocatalytic activity · Hydrophilic coatings

## Highlights

- Coupling  $\text{WO}_3$  with  $\text{SiO}_2$  and  $\text{ZnO}$  provided enhancement in the photocatalytic activity.
- The photocatalytic dye removal efficiency was improved to over 90% with  $\text{SiO}_2/\text{WO}_3/\text{ZnO}$  film under UVA light irradiation.
- The light transparency of the  $\text{SiO}_2/\text{WO}_3/\text{ZnO}$  film in the visible light spectrum was almost 5% lower than that of the cover glass of a solar cell.
- There was a decrease in the water contact angle due the photocatalytic degradation of the model contamination on the film coating under the UVA light irradiation.

## 1 Introduction

Self-cleaning coatings are found in a wide variety of applications such as solar cell panels, electronic and optical device panels, window glass, textiles and paints. Self-cleaning coatings contribute to reducing the efficiency lost of the solar cell, cleaning costs and maintaining stability of all surfaces. Self-cleaning coatings fall into two categories: hydrophobic and hydrophilic coatings [1]. A surface with a water contact angle greater than  $90^\circ$  is considered as hydrophobic. On the hydrophobic surfaces, water droplets take the shape of a sphere and clean the surface by rolling the formed droplets [2]. On the other hand, for hydrophilic surfaces with a water contact angle less than  $90^\circ$ , the self-cleaning mechanism occurs by photocatalytic degradation of the pollutants under UV radiation and then the removal of the contaminations formed on the surface with water. Semiconductor photocatalysts such as  $\text{ZnO}$  and  $\text{TiO}_2$  can be added to the surface coatings to make the surface hydrophilic [2, 3]. Photocatalytic degradation, which is part of the self-cleaning process on hydrophilic surfaces, is the decomposition of organic compounds into small molecules such as  $\text{CO}_2$  and  $\text{H}_2\text{O}$ . In photocatalytic degradation reactions, light with energy equal to or greater than the optical

band gap energy of the photocatalyst can be absorbed by the photocatalyst. In this case, electrons in the valence band of the photocatalyst are excited and transferred to the conduction band. The electron vacancies, called as holes ( $h^+$ ), are formed in the valence band of the photocatalyst, which can oxidize the surface adsorbed water molecule and turn it into a hydroxyl radical; the electrons excited to the conduction band can reduce the surface adsorbed  $\text{O}_2$  molecule and convert it to a superoxide radical. Both active radicals formed allow the degradation of organic pollutants adsorbed to the surface of the solar cell panel [2].

In the literature, different semiconductor photocatalysts such as  $\text{TiO}_2$  [4],  $\text{ZnO}$  [2],  $\text{KWO}_3$  [5] and  $\text{Bi}_2\text{O}_2\text{CO}_3$  [6] have been used to develop self-cleaning coatings based on the photocatalytic activity. Several studies from the literature have been summarized on Table 1. Self-cleaning by semiconductors takes place through the photocatalytic and the hydrophilicity mechanisms. The photocatalytic mechanism results to degradation of the pollution while the hydrophilicity mechanism laminates the water droplets on the surface to wash the degraded pollution, preventing the adhesion of the pollutants on the surface. In literature, Khorshidi and his coworkers (2021) measured the water contact angle on the acyclic/ $\text{ZnO}$  coating, deposited with a

**Table 1** Self-cleaning surface studies based on the photocatalytic activity from the literature

Coated Surface	Photocatalyst	Results
Building material (concrete surface) [6]	$\text{Bi}_2\text{O}_3$ , $\text{Bi}_2\text{O}_2\text{CO}_3$ , BiOI, $\text{BiVO}_4$ , $\text{BiPO}_4$	49% pollution (model dye) removal after 3 h with $\text{Bi}_2\text{O}_2\text{CO}_3$
Polymer (PMMA) [4]	$\text{TiO}_2$	Approximately 80% dye removal after 3 h
Glass surface [5]	$\text{KWO}_3$	29% dye removal after 2 h
Cement mortar [49]	$\text{TiO}_2/\text{ZnAl}$ layered double hydroxide	Reduction in water contact angle about $90^\circ$ in 210 min.
Glass surface [50]	$\text{WO}_3/\text{TiO}_2$	3.6% achievement in energy output gain after 8 months
Glass surface [10]	$\text{TiO}_2/\text{SiO}_2$	Reduction in water contact angle from $90^\circ$ to $20^\circ$ in 70 h.
Glass surface [51]	$\text{Cu-TiO}_2$ , $\text{Ag-TiO}_2$ , $\text{Fe-TiO}_2$ and $\text{Co-TiO}_2$	77, 74, 76 and 69% pollution (model dye) removal after 2 h with $\text{Cu-TiO}_2$ , $\text{Ag-TiO}_2$ , $\text{Fe-TiO}_2$ and $\text{Co-TiO}_2$
Glass surface [2]	Acrylic/ $\text{ZnO}$	Reduction in water contact angle from $90.2^\circ$ to $68.1^\circ$ in 135 min.
Glass surface [52]	$\text{TiO}_2/\text{Kaolin}$	65% dye removal after 210 min.

model pollutant (stearic acid). Under the UV light, the stearic acid molecules degraded into  $\text{H}_2\text{O}$  and  $\text{CO}_2$ .  $\text{H}_2\text{O}$  as a degradation product might decrease the water contact angle of the coating about  $22^\circ$  in 135 min. Hence, a decrease in the water contact angle might exhibit the potential of the photocatalytic activity and the cleaning of the coating surface [2].

The change in hydrophilic property of a solid surface with light radiation is related to the change in surface energy. There are different assumptions about determining the reasons of changes in surface energy at the atomic level. According to an assumption, the hydrophilic property of the solid surface increases with the contribution of organic pollution products that decompose under light. This is explained by the formation of metastable nano-sized hydrophilic regions on the surface due to the transport of the photogenerated electron-hole pairs to the solid surface. The second hypothetical mechanism of the photo-induced hydrophilic transformation of a surface is related to the thermal effect of light. This effect causes water bound by weak bonds in the outer layers of the solid surface to separate from the surface. Thus, the surface energy and thus the hydrophilicity of the solid increases. Then, water molecules spread on the solid surface, forming a film layer. Re-adsorption of water restores the initial structure of the hydrated layer and thus reduces the surface energy [7].

The sun provides free heat and electricity for real-life applications. In addition, the solar energy is environmentally friendly and it does not produce any emissions. For this reason, solar energy could be the most suitable and sustainable solution to the energy crisis of the World. However, several problems hinder optimum power harvesting from the photovoltaic (PV) modules. Dust accumulation on the surface of the PV module has been known as one of the crucial problems of the PV systems [8, 9]. As it is known, the light-permeable surface of the solar cell can be easily contaminated due to the adhesion of dust, organic

pollutants and inorganic particles. Accordingly, the light transmittance of the surface and the light absorption of the solar cell could reduce. In addition, cleaning the contaminated surface requires extra labor and money. There is also the possibility of scratching and damaging the surface during the cleaning. Therefore, the removal of the surface adsorbed pollution from the PV panel is of great importance [5]. There are three different self-cleaning methods, applied to clean the PV panels. Electrostatic, mechanical and coating methods are among these techniques to clean the surfaces of the PV panels, which are exposed to the outdoor conditions. The electrostatic method throws out the dust from the surface through the electrostatic wave. The mechanical method consists of four techniques, robotic method, air blowing method, water blowing method and ultrasonic vibration method, to expel surface adsorbed dust. The coating method technology is based on forming a thin layer of film coating, which can be either hydrophilic or hydrophobic. The hydrophilic coating reduces the surface pollution through a photocatalytic degradation reaction, while the hydrophobic coating rolls the water droplet to remove the pollution from the surface of the PV panel [8]. The accumulation of the pollution and its effect on the efficiency of the PV cell depends on the tilt angle of the PV system, the exposure duration, the climate conditions like the wind condition, the pollution density and the surface material of the PV system [10, 11].

Tungsten oxide ( $\text{WO}_3$ ) has been utilized as a photocatalyst for the degradation of the organic pollutants under the UV light irradiation.  $\text{WO}_3$  as a photocatalyst has important features like nontoxicity and chemical stability. Also,  $\text{WO}_3$  exhibits high resistance against acids and it has high photocorrosion resistance [12]. Due to the specified properties,  $\text{WO}_3$  is preferred in gas sensors, photochromic and electrochromic device applications.  $\text{WO}_3$  can also be thought as an appropriate anode material in the photoelectrochemical water splitting reactions [13]. Although  $\text{WO}_3$

can absorb the entire range of the UV light spectrum, the recombination rate of the photoinduced charge carriers, generated on  $\text{WO}_3$ , is high [14]. Forming a p-n heterojunction within the composite structure is a best solution to suppress the recombination of the photoinduced charge carriers and subsequently to enhance the photocatalytic activity. When n type and p type semiconductors are brought together to provide a stable contact, an electric field will be generated between the semiconductors, providing the reverse transfer of the charge carriers. The electric field provides the separation of the photoinduced charge carriers between the semiconductors [15]. In literature, several studies have been conducted to promote the separation of the photogenerated electron-hole pairs on  $\text{WO}_3$  such as  $\text{WO}_3/\text{TiO}_2$  [16],  $\text{WO}_3/\text{SnS}_2$  [17],  $\text{WO}_3/\text{SiO}_2$  [18],  $\text{WO}_3/\text{CdS}$  [19]. By coupling  $\text{WO}_3$  with another semiconductor possessing a valence band edge and a conduction band edge more positive or more negative in level than the valence band edge or the conduction band edge of  $\text{WO}_3$ , the photoexcited holes or electrons can move between the bands of the semiconductor and  $\text{WO}_3$ , suppressing the recombination of the photoinduced charge carriers on the semiconductor and  $\text{WO}_3$ . This event can enhance the photocatalytic activity [20]. In the scope of the study,  $\text{WO}_3$  was combined with  $\text{SiO}_2$  in the composite film structure. The sol-gel technique, known as one of the most efficient methods to prepare the composite films, was applied to prepared  $\text{SiO}_2/\text{WO}_3$  composite films. The sol-gel technique is relatively simple and a low-cost process when compared with the deposition methods applied under vacuum [21]. Also, ZnO was added into the composite film to enhance the photocatalytic activity and subsequently the self-cleaning property. The application potential of  $\text{SiO}_2/\text{WO}_3$  and  $\text{SiO}_2/\text{WO}_3/\text{ZnO}$  films as a self-cleaning coating on a real solar cell was studied. There were some challenges to be removed before the self-cleaning coatings could be used in practical application. ZnO and  $\text{WO}_3$  exhibit the light-induced superhydrophilicity and these semiconductors exhibit photocatalytic activity under UV light irradiation. When exposed to the UV light, ZnO or  $\text{WO}_3$  can degrade any kinds of organic contaminants or pollution adhering to the surface of the glass cover of the PV panel. The UV-induced superhydrophilic property of ZnO and  $\text{WO}_3$  allows water droplets to spread and flow on the surface of the cover glass, contributing to the self-cleaning process. Combining the self-cleaning process and the photocatalytic activity within a coating is of great importance in terms of the solar energy technology [21]. However, ZnO or  $\text{WO}_3$  coatings on the glass cover of the PV panel could reduce the transmittance owing to their relatively high refractive index ( $n = 2$  for ZnO and  $n = 1.9$  for  $\text{WO}_3$ ) compared to  $\text{SiO}_2$  ( $n = 1.5$ ) [22]. On the other hand,  $\text{SiO}_2$  with a low refractive index and low surface scattering is beneficial and effective in improving

the light transmission for the glass cover of the PV panel. In addition,  $\text{SiO}_2$  film exhibits hydrophilicity and self-cleaning properties owing to the presence of hydroxyl groups in its chemical structure [21]. However, the superhydrophilicity of a  $\text{SiO}_2$  film coated on the cover glass of the PV panel may reduce in time owing to deposition of dust and organic pollutants, and the photocatalytic activity of  $\text{SiO}_2$  is low [22]. The optimization of the coated film in terms of the specified features is a significant and a detailed study was conducted to achieve a balance between the specified properties. In literature, there is no study on the self-cleaning effect of  $\text{SiO}_2/\text{WO}_3/\text{ZnO}$  films for solar cells.

## 2 Experimental

### 2.1 Materials and methods

$\text{SiO}_2$ ,  $\text{WO}_3$  and ZnO solutions were prepared separately to prepare  $\text{SiO}_2/\text{WO}_3$  and  $\text{SiO}_2/\text{WO}_3/\text{ZnO}$  films. To prepare the  $\text{SiO}_2$  solution, tetraethylorthoxylsilicane (TEOS) (112 ml, 0.5 mol,  $\geq 97.5\%$ , ISOLAB) was mixed with a certain amount of distilled water-anhydrous ethanol solution (36 ml, 2 mol–1090 ml, 18.7 mol). Then, concentrated hydrochloric acid solution ( $\sim 0.2$  ml, 36%, 2.3 mmol) was added into the solution to obtain a final molar ratio of TEOS : ethyl alcohol :  $\text{H}_2\text{O}$  :  $\text{HCl}$  as 1 : 37.5 : 4 : 0.004. The expected concentration of  $\text{SiO}_2$  within the final solution was 3 wt.%. The solution was stirred in a closed glass vessel at the room temperature for 2 h and held in the dark for 1 day [23]. To prepare the  $\text{WO}_3$  solution, sodium tungstate dihydrate ( $\text{Na}_2\text{WO}_4 \cdot 2\text{H}_2\text{O}$ , ACS reagent, Sigma-Aldrich) (3 g) was dissolved in 20 ml of distilled water and stirred at the room temperature. HCl solution (20 ml, 8 M, 0.16 mol) was added into the prepared solution. Then, the solution was stirred for 2 h at 80 °C. After cooling to room temperature, the as-prepared solution was held in the dark for 1 day [24]. On the other hand, zinc acetate 2-hydrate ( $\text{Zn}(\text{CH}_3\text{COO})_2 \cdot 2\text{H}_2\text{O}$ , ACS reagent, Sigma-Aldrich) was used as a precursor of Zn atom to prepare the ZnO solution. Absolute ethanol (ACS, ISO, Reagent, ISOLAB) and diethanolamine (reagent grade, Sigma-Aldrich) were used as a solvent and a solution stabilizer, respectively. In detail, 0.05 mol of  $\text{Zn}(\text{CH}_3\text{COO})_2 \cdot 2\text{H}_2\text{O}$  was dissolved in ethanol (100 ml, 1.7 mol) to obtain 0.5 M solution. The as-prepared solution was stirred for half an hour. Then, 0.05 mol of the solution stabilizer was added into the solution under stirring. Afterward, the solution was stirred for 30 min. The as-prepared solution was held in the dark for 1 day [25].

The  $\text{SiO}_2$  solution and the  $\text{WO}_3$  solution was mixed with varying ratios (80/20, 70/30, 60/40, 50/50, 40/60, 30/70 and 20/80 wt./wt.) to obtain the  $\text{SiO}_2/\text{WO}_3$  composite solutions. The composite solutions were stirred for 2 h and held in the

dark for 1 day. Within the scope of the optimization study, the optimum SiO<sub>2</sub>/WO<sub>3</sub> composition was determined by using the photocatalytic activity measurements. The SiO<sub>2</sub>/WO<sub>3</sub> film composition, resulted the highest photocatalytic activity, was determined and the optimum SiO<sub>2</sub>/WO<sub>3</sub> composition was used in the remaining studies to prepare the SiO<sub>2</sub>/WO<sub>3</sub>/ZnO composites. In addition, the ZnO solution was mixed with varying ratios ((SiO<sub>2</sub>/WO<sub>3</sub>)/ZnO : 70/30, 80/20 and 90/10 wt./wt.) with the optimum SiO<sub>2</sub>/WO<sub>3</sub> solution to prepare the SiO<sub>2</sub>/WO<sub>3</sub>/ZnO composites. The composite films were labeled as SiO<sub>2</sub>/WO<sub>3</sub>(x/y) based on the weight ratio of SiO<sub>2</sub> to WO<sub>3</sub>. In addition, the composite films were labeled as SiO<sub>2</sub>/WO<sub>3</sub>/ZnO(x/y) based on the weight ratio of SiO<sub>2</sub>/WO<sub>3</sub> to ZnO. Ultrasonic cleaning was applied to the glass substrates in acetone prior to the dip-coating process. The as-prepared solutions were deposited on the glass substrates through the dip-coating technique at the ambient condition. A constant withdraw speed (100 mm/min) was applied during the dip-coating process. After the dip-coating process, the glass substrate was dried at the ambient condition for 2 h. The as-deposited film was pre-heated at 100 °C for 1 h to remove the unreacted volatile species. Afterward, it was annealed at 400 °C for 2 h to provide the growth of the crystalline phase [23]. As a process parameter, the number of the dip-coating cycle was changed to investigate the effect of the film thickness on the photocatalytic activity, the light transmittance ratio and the efficiency loss of the solar cell.

## 2.2 Structural, morphological and optical characterization

Fourier transform infrared (FTIR) spectra of the film samples was obtained by scanning between the wavenumber range of 4000–400 cm<sup>-1</sup> using a Bruker IFS 66/S model FTIR spectrophotometer with a resolution of 4 cm<sup>-1</sup>. It was planned to evaluate the chemical bond structures of the photocatalyst systems using the FTIR spectroscopy. X-ray diffraction (XRD) patterns of the film samples was recorded to identify the crystal structure. A Rigaku Ultima IV model X-ray diffractometer was used with monochromatic Cu K $\alpha$  radiation ( $\lambda = 1.5406 \text{ \AA}$ ) at a scan rate of 1°/min. The morphology of the coated films was examined with a QUANTA 400 F field emission scanning electron microscope (FESEM). A conductive coating was deposited on the samples prior to the analysis. The distribution and the interaction of the composite constituents within the composite structure was examined using the FESEM images. The elemental composition of the film samples was investigated by energy dispersive X-ray (EDX) spectroscopy (JXA-8230 EDX Microanalysis Instrument).

The transmittance and absorbance spectrum of the coated films were recorded in the wavelength range of 200–800 nm

using a Genesys 10 S (Thermo Scientific) model spectrophotometer. The UV-Vis absorbance spectrum was used to determine the optical band gap of the coated film by using the Tauc equation given below [2]:

$$\alpha h\nu = A(h\nu - E_g)^{1/2} \quad (1)$$

at which  $\alpha$ ,  $E_g$  and  $h\nu$  are the absorption coefficient, the optical band gap energy and the photon energy, respectively. The optical band gap energy was estimated by extrapolating the linear part of the curve to the x-axis on the plot of  $(\alpha h\nu)^2$  vs.  $h\nu$ . The film thickness was calculated using the transmittance spectrum of the as-prepared film samples through the following equation [26]:

$$d = 1/n(\lambda/4(2m + 1)) \quad (2)$$

at which  $d$  is the film thickness, where  $m$  ( $=0, 1, 2, 3, \dots$ ) is the order of the minimum transmittance ( $T_{\min \text{ abs}}$ ) and  $n$  is the refractive index. The refractive index ( $n$ ) at the absolute minimum transmittance ( $T_{\min \text{ abs}}$ ) was calculated using the following equation [26]:

$$n = ((n_0 n_2)^{0.5})(1 + (1 - T_{\min \text{ abs}})^{0.5}) / (T_{\min \text{ abs}})^{0.5} \quad (3)$$

where  $n_0$  ( $n_0 = 1$ ) is the refractive index of air and  $n_2$  ( $n_2 = 1.515$ ) is the refractive index of the glass plate.

The film coatings should not reduce the efficiency of the solar cell due to a possible decrease in the solar light transmittance. The negative effects of self-cleaning coatings on the efficiency of the solar cell was also examined in the scope of this study. Most of the studies conducted on the self-cleaning coatings for the PV system have neglected to measure the efficiency loss that might occur in the solar cell. The efficiency of the self-cleaning coated solar cell and the uncoated solar cell was compared. The efficiency of a solar cell was calculated using the following equation:

$$\eta(\text{efficiency}) = V_{OC} I_{SC} FF / P_{in} \quad (4)$$

where  $V_{OC}$  is the open-circuit voltage,  $I_{SC}$  is the short-circuit current and  $FF$  is the fill factor. The glass substrate coated with the self-cleaning coating was placed on the top of a solar cell and the efficiency of this solar cell was measured. As a reference, an uncoated glass substrate was also placed on the top of the solar cell and its efficiency was measured.

## 2.3 Characterization of the photocatalytic activity and the self-cleaning performance

The photocatalytic activity of the as-prepared coatings, soiled with a model organic compound (methylene blue),



was monitored under UVA light irradiation (12 W). For this purpose, the coated film samples were immersed into the methylene blue solution (10 mg/l) and then dried in the air atmosphere. The coatings adsorbed with methylene blue was irradiated with UVA light and at certain time intervals (30 min.), the degradation of methylene blue on the coatings was evaluated by measuring the reduction in the absorbance maximum peak of the model compound (664 nm) using a Genesys 10 S model (Thermo Scientific) spectrophotometer by the following equation [5]:

$$\text{Degradation efficiency (\%)} = (A_0 - A)/A_0 \quad (5)$$

where  $A_0$  is the initial absorbance of methylene blue and  $A$  is the absorbance of methylene blue after the UV light irradiation. The average result of three dye degradation measurements was reported for each film. For comparison purposes, the photocatalytic activity of the optimum  $\text{SiO}_2/\text{WO}_3$  film, soiled with methylene blue, was also monitored under visible light irradiation (300 W, Osram Ultravitalux). The two most conventional techniques to investigate the photocatalytic self-cleaning property of the coated film are the dye method and the stearic acid method. In both methods, the dye and the stearic acid are considered as organic contamination, and the decomposition process of the organic contaminants under UV radiation can be studied to analyze the self-cleaning process. For this purpose, the water contact angle can be measured for the film coated with the organic dye or the fatty acid (stearic acid) [2, 27]. The photocatalytic self-cleaning activity of the optimum  $\text{SiO}_2/\text{WO}_3$  and  $\text{SiO}_2/\text{WO}_3/\text{ZnO}$  films was analyzed using the water contact angle measurement following the dye method. According to the dye method, methylene blue was dissolved in distilled water (10 mg/l) and it was tried to be adsorbed on the coated films by the dip coating technique. The sample containing the organic pollutant was then exposed to the UVA light. The degradation of the organic pollutant was observed by measuring the water contact angle on the glass surface at certain time intervals (30 min). The contact angle measurement of the water drop was

performed at 3 different points on the coating surface according to the fixed drop (sessile drop) method using an optical tensiometer (Theta Lite, Biolin Scientific). Average result of three measurements was reported for each film [27].

## 3 Results and discussion

### 3.1 FTIR analysis

As illustrated in Fig. 1a, FTIR absorbance spectrum confirmed the successful synthesis of  $\text{SiO}_2$ . There is a broad band on the FTIR spectrum of  $\text{SiO}_2$  from 2800 to 3800  $\text{cm}^{-1}$ , assigned to the presence of the O-H group [28]. In addition, there is a weak absorbance peak at 1623  $\text{cm}^{-1}$ , assigned to the O-H stretching bond [28]. On the other hand, there are strong absorbance peaks at 453, 819 and 1074  $\text{cm}^{-1}$ , attributed to the asymmetric and symmetric Si-O-Si stretching vibrations [28, 29]. The weak absorbance peak at 1378  $\text{cm}^{-1}$  might be due to the C-H bond of the  $\text{SiO}_2$  precursor (TEOS) [29]. On the FTIR spectrum of pure  $\text{WO}_3$  film (Fig. 1b), there is a broad absorbance band at around 590  $\text{cm}^{-1}$  and a sharp absorbance peak at around 800  $\text{cm}^{-1}$ , which were attributed to the  $\text{W}=\text{O}$  stretching bond and the O-W-O stretching bond, respectively [30]. FTIR spectrum of pure ZnO film illustrates characteristic peak of ZnO at 482 and 555  $\text{cm}^{-1}$ , which were attributed to the Zn-O stretching vibrations (Fig. 1c) [31]. In addition, there are additional peaks at 865, 1039, 1392 and 1629  $\text{cm}^{-1}$ , which were assigned to the symmetric bending of the H-O-H bond, the stretching vibration of the C-O bond of the primary alcohol, the secondary alcohol vibration and the vibration mode of alkyls, respectively [31, 32]. Also, there is a wide absorbance band at around 3438  $\text{cm}^{-1}$  and peaks at 2896, 2975  $\text{cm}^{-1}$  due to the stretching vibration of hydroxyl compounds [31, 32].

In Fig. 1d, FTIR absorbance spectrum of the composite film sample confirmed the successful synthesis of both  $\text{SiO}_2$  and  $\text{WO}_3$  together. The characteristic absorbance peaks of

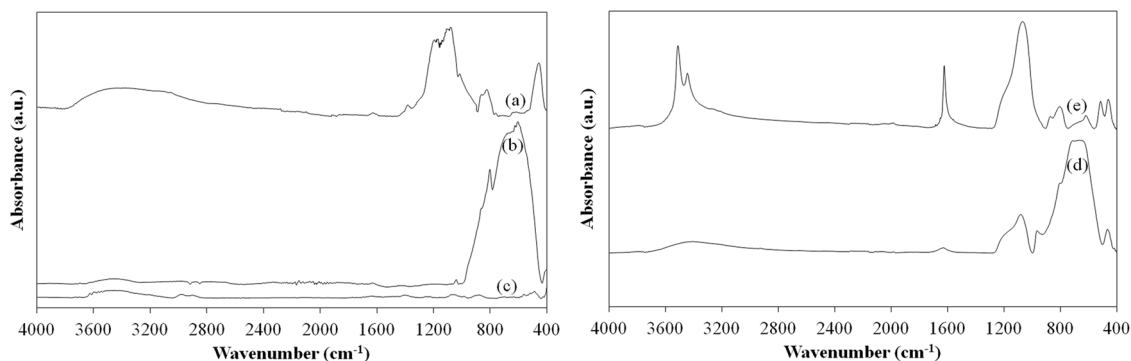


**Fig. 1** FTIR spectrum of (a)  $\text{SiO}_2$ , (b)  $\text{WO}_3$ , (c) ZnO, (d)  $\text{SiO}_2/\text{WO}_3(30/70)$  and (e)  $\text{SiO}_2/\text{WO}_3/\text{ZnO}(70/30)$  films

$\text{WO}_3$  were observed at  $667$  and  $966\text{ cm}^{-1}$ , assigned to the  $\text{W}=\text{O}$  stretching bond [30]. The spectrum also presents the characteristic peak of  $\text{WO}_3$  at  $957\text{ cm}^{-1}$ , belonging to the stretching of short  $\text{W}=\text{O}$  bonds of  $\text{WO}_3\cdot\text{H}_2\text{O}$ . On the other hand, the characteristic peaks of  $\text{SiO}_2$  were observed at  $467$ ,  $797$  and  $1083\text{ cm}^{-1}$ , attributed to the  $\text{Si}-\text{O}-\text{Si}$  stretching vibrations [28, 29]. In addition, there is a weak absorbance peak at  $1629\text{ cm}^{-1}$ , which was attributed to the  $\text{Si}-\text{OH}$  vibrations [29]. FTIR spectrum exhibits a broad band at around  $3410\text{ cm}^{-1}$  due to the  $\text{O}-\text{H}$  group [28]. On the FTIR spectrum of the  $\text{SiO}_2/\text{WO}_3/\text{ZnO}(70/30)$  (Fig. 1e), the characteristic absorbance peak of  $\text{SiO}_2$  due to the  $\text{Si}-\text{O}-\text{Si}$  stretching vibrations appears at  $463$  and  $1067\text{ cm}^{-1}$ , respectively [28, 29]. The peak present at  $515\text{ cm}^{-1}$  might belong to the  $\text{Zn}-\text{O}$  stretching vibrations [31]. Characteristic peaks of  $\text{WO}_3$  due to the  $\text{W}=\text{O}$  stretching bond and the  $\text{O}-\text{W}-\text{O}$  stretching bond are present at  $620$  and  $806\text{ cm}^{-1}$ , respectively, on the same spectrum [30]. On the spectrum, there are additional peaks at  $871$ ,  $1624$ ,  $3445$  and  $3512\text{ cm}^{-1}$ , which were attributed to the stretching vibration of hydroxyl compounds [28, 31, 32].

### 3.2 XRD analysis

The XRD analysis was conducted to investigate the crystal structure of pure and composite film samples. Figure 2a illustrates the XRD pattern of the  $\text{SiO}_2$  film. The XRD profile of the  $\text{SiO}_2$  film exhibited a broad peak at round  $23^\circ$  owing to the formation of amorphous  $\text{SiO}_2$  nanoparticles [33]. According to Fig. 2b, all the peaks on the XRD pattern, in well accordance with the JCPDS No. 83-0950, might be consigned to the monoclinic  $\text{WO}_3$  crystal phase. The more intense peaks at  $23.6^\circ$ ,  $24.3^\circ$ ,  $26.6^\circ$ ,  $28.8^\circ$ ,  $34.1^\circ$ ,  $41.9^\circ$ ,  $48.4^\circ$ ,  $49.9^\circ$  and  $55.8^\circ$  corresponding to the (002), (200), (120), (112), (202), (222), (040), ( $-114$ ) and (142) planes provided a strong evidence for the monoclinic  $\text{WO}_3$  phase [34]. Figure 2c illustrates the XRD pattern of pure ZnO film. The peaks of the ZnO film belongs to the typical hexagonal wurtzite structure. The diffraction pattern

exhibited sharp and intense peaks at  $31.9^\circ$ ,  $34.5^\circ$ ,  $36.4^\circ$ ,  $47.7^\circ$ ,  $56.7^\circ$ ,  $63.0^\circ$  and  $68.1^\circ$  corresponding to the (100), (002), (101), (102), (110), (103) and (112) planes of the ZnO phase, respectively (JCPDS No. 36-1451) [35]. No impurity phase was observed for pure ZnO, revealing the successful synthesis of ZnO in the film structure.

Figure 2d shows the XRD pattern of the  $\text{SiO}_2/\text{WO}_3(30/70)$  film sample. The XRD pattern exhibited characteristic peaks of the  $\text{WO}_3$  phase corresponding to the (002), (200), (120), (112), (202), (222), (040), ( $-114$ ), (142) and (142) planes at the diffraction angle of  $23.6^\circ$ ,  $24.3^\circ$ ,  $26.6^\circ$ ,  $28.6^\circ$ ,  $34.1^\circ$ ,  $41.8^\circ$ ,  $48.3^\circ$ ,  $49.9^\circ$ ,  $55.7^\circ$  and  $56.4^\circ$ , respectively [34]. The broad peak belonging to the amorphous  $\text{SiO}_2$  structure could not be detected on the XRD pattern of the composite film. Within the composite structure, the amorphous  $\text{SiO}_2$  phase might be converted to the crystalline phase. According to the standard card of the crystalline  $\text{SiO}_2$  (JCPDS data of 46-1045), there are two characteristic peaks of  $\text{SiO}_2$  at  $21.1^\circ$  and  $26.6^\circ$  [36]. The peak at  $21.1^\circ$  was not present on the XRD pattern of the composite film sample. The peak at  $26.6^\circ$  might be lost in the peak of  $\text{WO}_3$  at  $26.6^\circ$ . When compared with pure  $\text{WO}_3$ , there was a slight shift in the peak position toward the side of smaller diffraction angle with the composite film structure. Figure 2e illustrates the XRD pattern of the  $\text{SiO}_2/\text{WO}_3/\text{ZnO}(70/30)$  film sample. The XRD pattern exhibited characteristic peaks of the  $\text{WO}_3$  phase corresponding to the (002), (200), (120), (112), (222), (040), ( $-114$ ) and (142) planes at  $2\theta$  values of  $23.8^\circ$ ,  $24.5^\circ$ ,  $25.9^\circ$ ,  $29.9^\circ$ ,  $41.3^\circ$ ,  $48.3^\circ$ ,  $48.7^\circ$  and  $55.6^\circ$ , respectively [34]. The same pattern included characteristic peaks of the ZnO phase at  $31.2^\circ$ ,  $33.6^\circ$ ,  $36.6^\circ$ ,  $47.7^\circ$ ,  $64.7^\circ$  and  $68.2^\circ$  [35]. The characteristic peak belonging to the crystalline  $\text{SiO}_2$  phase was present at  $21.1^\circ$ , suggesting that the amorphous  $\text{SiO}_2$  phase was converted to the crystalline phase [36].

### 3.3 Morphological analysis

Figure 3 shows the FESEM images of pure  $\text{SiO}_2$ , pure  $\text{WO}_3$  and pure ZnO film samples. Pure  $\text{SiO}_2$  film is homogeneous

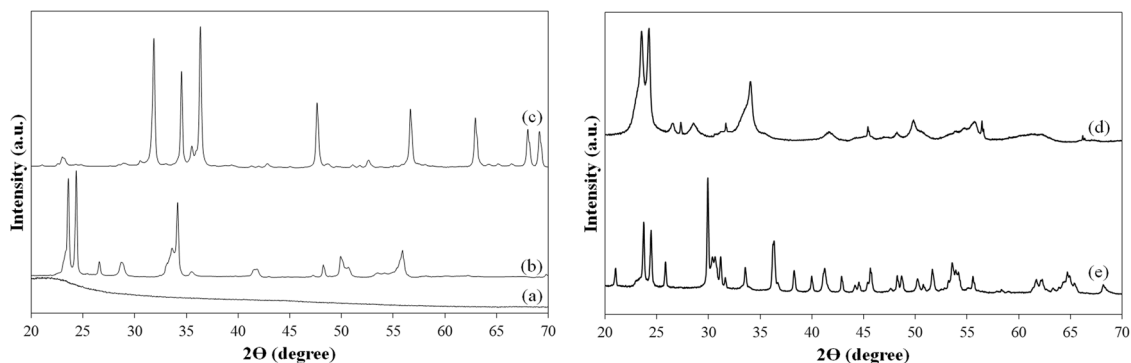


**Fig. 2** XRD spectrum of (a)  $\text{SiO}_2$ , (b)  $\text{WO}_3$ , (c) ZnO, (d)  $\text{SiO}_2/\text{WO}_3(30/70)$  and (e)  $\text{SiO}_2/\text{WO}_3/\text{ZnO}(70/30)$  films

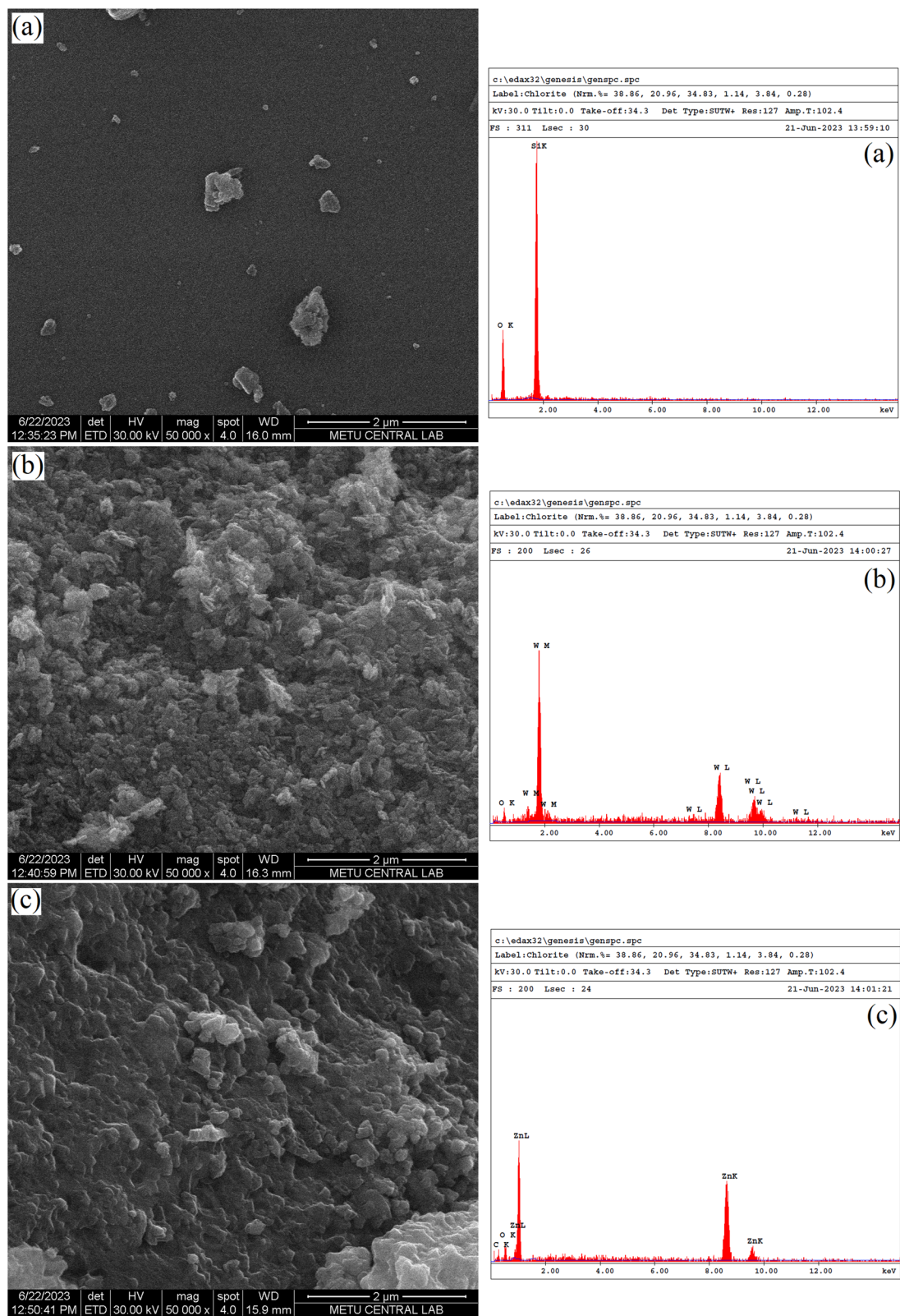


Fig. 3 FESEM image and EDX spectrum of (a) SiO<sub>2</sub>, (b) WO<sub>3</sub> and (c) ZnO films



and without cracks over a wide area. In addition, the  $\text{SiO}_2$  film has a smooth surface area. On the other hand, there is no smooth surface area with the  $\text{WO}_3$  and ZnO films. There was a significant grain growth on the  $\text{WO}_3$  and ZnO film surfaces. The crystal grains were less tightly packed on both of the film surfaces. When compared with the  $\text{WO}_3$  film surface, the surface of the ZnO film seems to be smoother. Figure 3 also shows the EDX spectrum of pure  $\text{SiO}_2$ , pure  $\text{WO}_3$  and pure ZnO film samples. The EDX spectroscopy proved the successful synthesis of  $\text{SiO}_2$ ,  $\text{WO}_3$  and ZnO films from their precursor solutions.

Figure 4 illustrates the FESEM images of the  $\text{SiO}_2/\text{WO}_3(30/70)$  film and the  $\text{SiO}_2/\text{WO}_3/\text{ZnO}(70/30)$  film

samples. The surface structure of the  $\text{SiO}_2/\text{WO}_3(30/70)$  film is similar to the surface structure of pure  $\text{WO}_3$  film. There was also a significant grain growth on the composite film surface. The grain structure might belong to the  $\text{WO}_3$  phase of the composite film. Compared to pure  $\text{WO}_3$  film, the grain structures seem to be smaller. As the  $\text{WO}_3$  phase was the dominant phase in the composite, smooth surface areas belonging to the  $\text{SiO}_2$  phase were not obvious on the FESEM image of the  $\text{SiO}_2/\text{WO}_3(30/70)$  film sample. The  $\text{SiO}_2$  phase might be embedded into the  $\text{WO}_3$  phase, forming a homogeneous  $\text{SiO}_2/\text{WO}_3$  film layer. On the FESEM image of the  $\text{SiO}_2/\text{WO}_3/\text{ZnO}(70/30)$  film, there was also a significant grain growth. There are two different grain

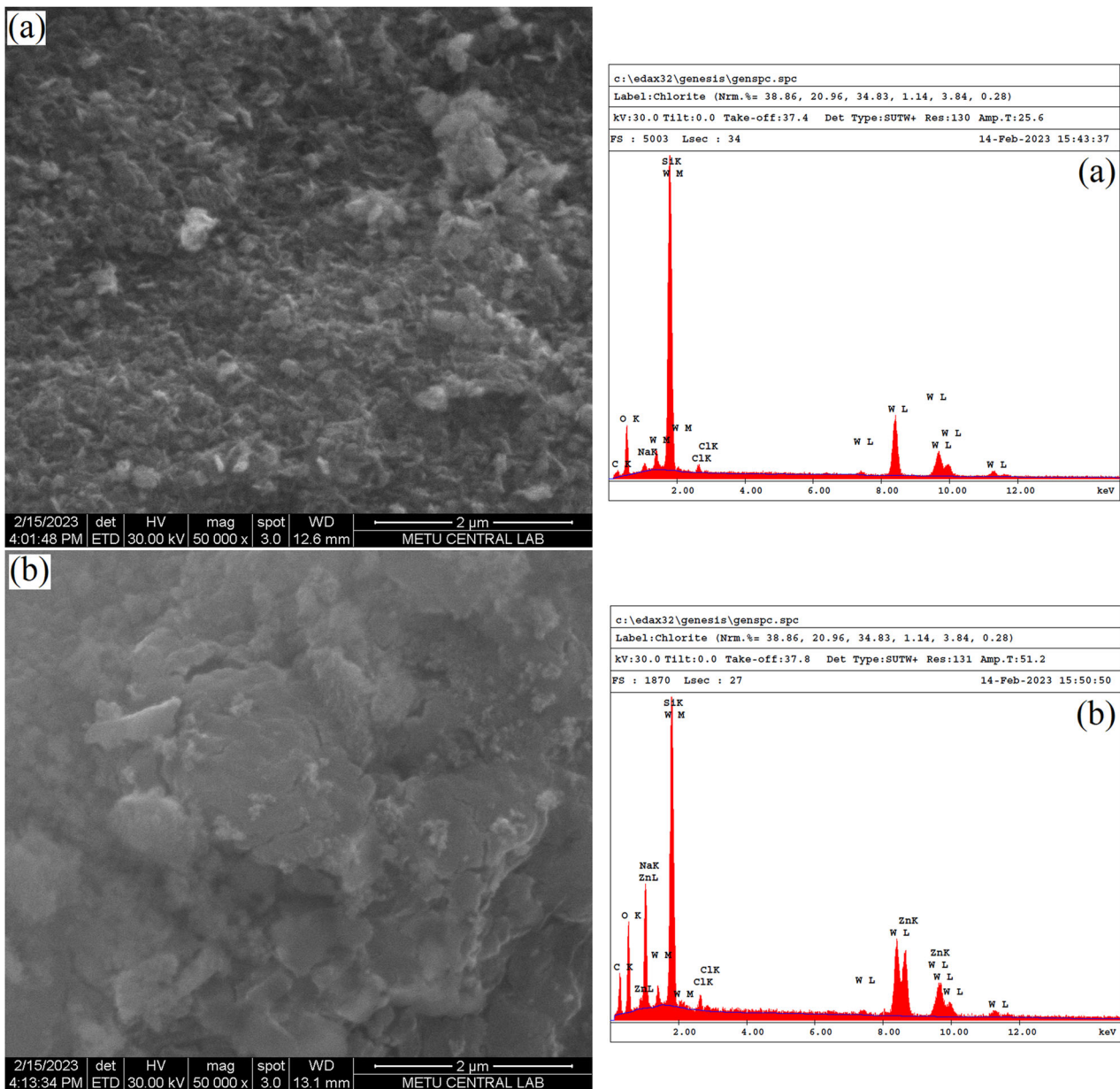
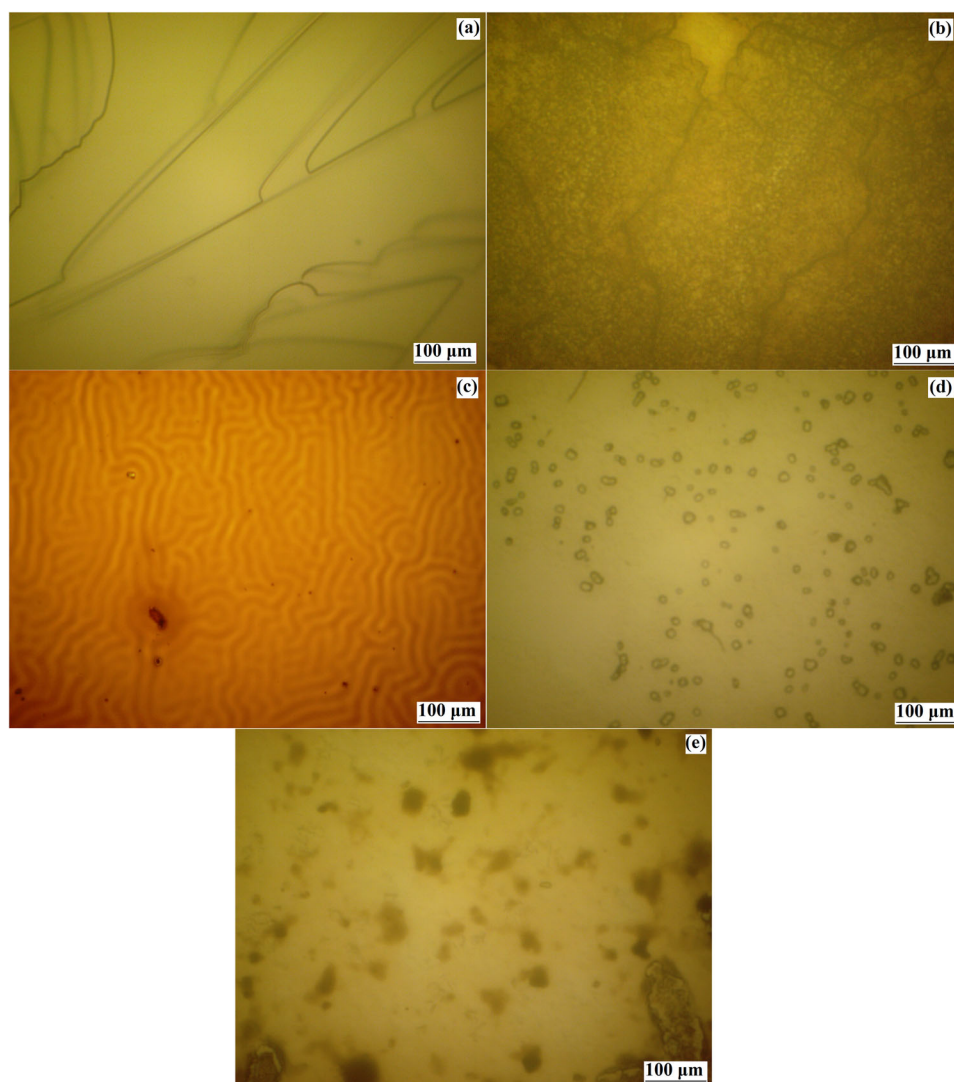


Fig. 4 FESEM image and EDX spectrum of (a)  $\text{SiO}_2/\text{WO}_3(30/70)$  and (b)  $\text{SiO}_2/\text{WO}_3/\text{ZnO}(70/30)$  films

**Fig. 5** Optical microscopy image of (a) SiO<sub>2</sub>, (b) WO<sub>3</sub>, (c) ZnO, (d) SiO<sub>2</sub>/WO<sub>3</sub>(30/70) and (e) SiO<sub>2</sub>/WO<sub>3</sub>/ZnO(70/30) films



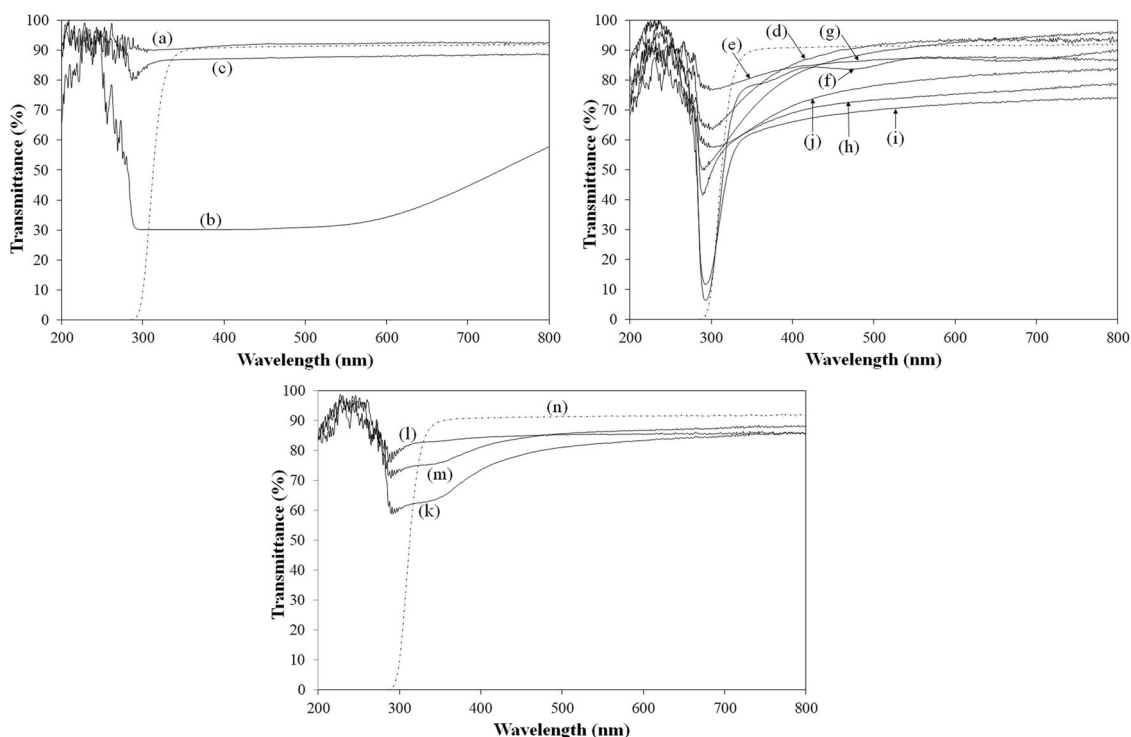
structures in two different sizes. The larger grain structures might belong to the ZnO phase and the smaller grain structure might belong to the WO<sub>3</sub> phase. Compared to the SiO<sub>2</sub>/WO<sub>3</sub>(30/70), the surface structure of the SiO<sub>2</sub>/WO<sub>3</sub>/ZnO(70/30) seems to be less smooth. EDX spectrum of the SiO<sub>2</sub>/WO<sub>3</sub>(30/70) film and the SiO<sub>2</sub>/WO<sub>3</sub>/ZnO(70/30) film samples exhibited all the elements of the composite constituents. According to the EDX spectra, both of the composite films were successfully prepared.

Figure 5 illustrates the optical microscopy image of the film samples. In all images, there are very few cracks. The cracks, which could occur during the dip coating and drying processes due to the removal of solvent at high speeds, might disappear during the annealing process at 400 °C. The dark spherical regions in the SiO<sub>2</sub>/WO<sub>3</sub>(30/70) film might belong to the WO<sub>3</sub> phase. The optical microscope images of pure SiO<sub>2</sub> and pure WO<sub>3</sub> films supported this idea. Pure SiO<sub>2</sub> film includes only crack and there are no dark

spherical regions. On the other hand, pure WO<sub>3</sub> film includes only a large dark region. According to the optical microscope images, smooth and homogeneous film surfaces were obtained. The optical microscope image of the SiO<sub>2</sub>/WO<sub>3</sub>/ZnO film is similar to the image of the SiO<sub>2</sub>/WO<sub>3</sub> film. As a difference, there are more dark regions in different sizes. Small-sized and large-sized regions might belong to the WO<sub>3</sub> and ZnO phases, respectively.

### 3.4 Light transmittance study

Figure 6 shows the light transmittance spectrum of the film samples. Pure WO<sub>3</sub> film exhibited low transmittance of about 44% between 300 and 800 nm, whereas pure SiO<sub>2</sub> film exhibited high transmittance (~92%) in the same region. Hence, an increase in the WO<sub>3</sub> content of the composite film resulted in a reduction in the average transmittance in the whole visible region (Fig. 6d–j). According to Fig. 6d,



**Fig. 6** Transmittance spectrum of (a) SiO<sub>2</sub>, (b) WO<sub>3</sub>, (c) ZnO, (d) SiO<sub>2</sub>/WO<sub>3</sub>(80/20), (e) SiO<sub>2</sub>/WO<sub>3</sub>(70/30), (f) SiO<sub>2</sub>/WO<sub>3</sub>(60/40), (g) SiO<sub>2</sub>/WO<sub>3</sub>(50/50), (h) SiO<sub>2</sub>/WO<sub>3</sub>(40/60), (i) SiO<sub>2</sub>/WO<sub>3</sub>(30/70), (j)

SiO<sub>2</sub>/WO<sub>3</sub>(20/80), (k) SiO<sub>2</sub>/WO<sub>3</sub>/ZnO(90/10), (l) SiO<sub>2</sub>/WO<sub>3</sub>/ZnO(80/20), (m) SiO<sub>2</sub>/WO<sub>3</sub>/ZnO(70/30) and (n) uncoated glass slide

uncoated glass slide transmitted more UVA light between 320 and 470 nm than the glass slide coated with the SiO<sub>2</sub>/WO<sub>3</sub>(80/20) film. The transparency of the SiO<sub>2</sub>/WO<sub>3</sub>(80/20) film in the visible light spectrum (above 470 nm) was almost 3% higher than that of uncoated glass slide. The reason for the enhancement in the transparency might be the reduced reflectance on the SiO<sub>2</sub>/WO<sub>3</sub>(80/20) film. Figure 6e, f exhibit the transmittance spectra of the SiO<sub>2</sub>/WO<sub>3</sub>(70/30) and SiO<sub>2</sub>/WO<sub>3</sub>(60/40) film samples. The average transmittance of the SiO<sub>2</sub>/WO<sub>3</sub>(70/30) and SiO<sub>2</sub>/WO<sub>3</sub>(60/40) film samples in the visible light range was almost 85 and 86%, respectively. As compared to uncoated glass slide (91%), the SiO<sub>2</sub>/WO<sub>3</sub>(70/30) and SiO<sub>2</sub>/WO<sub>3</sub>(60/40) film samples exhibited lower transmittance. The average light transmittance of the SiO<sub>2</sub>/WO<sub>3</sub>(50/50) film in the visible region was around 91%, which was almost the same light transmittance as the uncoated glass slide. The remaining film samples (SiO<sub>2</sub>/WO<sub>3</sub>(40/60), SiO<sub>2</sub>/WO<sub>3</sub>(30/70) and SiO<sub>2</sub>/WO<sub>3</sub>(20/80)) showed average transmittance between 77 and 70% in the visible light region (Fig. 6h–j).

The SiO<sub>2</sub>/WO<sub>3</sub>(30/70) composite film was also combined with ZnO during the dip coating process. Pure ZnO film exhibited nearly high light transmittance (~88%) in the visible light range as the uncoated glass slide. Hence, it was expected that the contribution of the ZnO phase into the SiO<sub>2</sub>/WO<sub>3</sub> composite structure might enhance the light transparency. As expected SiO<sub>2</sub>/WO<sub>3</sub>/ZnO film systems

provided higher transmittance than that of the SiO<sub>2</sub>/WO<sub>3</sub>(30/70) film sample (Fig. 6k). The SiO<sub>2</sub>/WO<sub>3</sub>/ZnO(90/10) has an average transmittance of 83% in the visible light region. The transmittance of the SiO<sub>2</sub>/WO<sub>3</sub>/ZnO film samples increased with the ZnO content. The SiO<sub>2</sub>/WO<sub>3</sub>/ZnO(80/20) and SiO<sub>2</sub>/WO<sub>3</sub>/ZnO(70/30) film samples achieved average transmittance of 85 and 87%, respectively (Fig. 6l, m). The absorber layer of the solar cell should have an optical band gap, optimized relative to the solar spectrum for maximum energy conversion through the photovoltaic effect. A narrow optical band gap increases the number of photons absorbed by the solar cell, while a wide optical band gap increases the useful energy obtained from each receiving photon. This leads to an optical band gap between 1.1 eV and 1.5 eV with a maximum solar-to-electrical power-conversion efficiency of ~30% for non-concentrated terrestrial solar illumination [37]. Hence, the film coating on the glass cover of the solar cell should have high transmittance between 1.1 eV and 1.5 eV (825 nm and 1125 nm). The light transmittance for the SiO<sub>2</sub>/WO<sub>3</sub> film samples varied between 74 and 96%, and the light transmittance for the SiO<sub>2</sub>/WO<sub>3</sub>/ZnO film samples varied 86 and 88% at 800 nm. Relatively high light transmittance at 800 nm was obtained with all film samples. The thickness of the coated film samples was estimated using the transmittance spectrum of the as-prepared samples following procedure of Salvaggio and his coworkers [26]. The calculated film thickness values, using the transmittance data, varied

between 10 and 100 nm for the  $\text{SiO}_2/\text{WO}_3$  and the  $\text{SiO}_2/\text{WO}_3/\text{ZnO}$  film samples (Table 2). There was no significant change in the film thickness depending on the composition both for the  $\text{SiO}_2/\text{WO}_3$  and the  $\text{SiO}_2/\text{WO}_3/\text{ZnO}$  film samples.

Within the scope of the optimization study, the number of the dip-coating cycle was changed to investigate the effect of the film thickness on the light transparency. Fig. S1 exhibits the transmittance spectra of the  $\text{SiO}_2/\text{WO}_3(30/70)$  film sample. The average transmittance of the  $\text{SiO}_2/\text{WO}_3(30/70)$  (1-fold coating),  $\text{SiO}_2/\text{WO}_3(30/70)$  (2-fold

coating) and  $\text{SiO}_2/\text{WO}_3(30/70)$  (3-fold coating) film samples in the visible light range was almost 72, 65 and 57%, respectively. In addition, the average transmittance of the  $\text{SiO}_2/\text{WO}_3/\text{ZnO}(70/30)$  (1-fold coating),  $\text{SiO}_2/\text{WO}_3/\text{ZnO}(70/30)$  (2-fold coating) and  $\text{SiO}_2/\text{WO}_3/\text{ZnO}(70/30)$  (3-fold coating) film samples in the visible light range was almost 87, 72 and 63%, respectively. When the number of the dip-coating cycle increased, the light transparency decreased for the film samples. With an increase in the number of the dip-coating cycle, the film thickness might increase or the film might turn into a denser structure.

**Table 2** The refractive index ( $n$ ) at the absolute minimum transmittance and the film thickness of the  $\text{SiO}_2/\text{WO}_3$  and  $\text{SiO}_2/\text{WO}_3/\text{ZnO}$  film samples calculated using the transmittance data

Sample	$\lambda$ (nm)	$T_{\min \text{ abs}}$	$n$	$d$ (nm)
$\text{SiO}_2/\text{WO}_3(80/20)$	298	0.63471	2.48	90.17
$\text{SiO}_2/\text{WO}_3(70/30)$	292	0.68155	2.33	93.90
$\text{SiO}_2/\text{WO}_3(60/40)$	293	0.0239	15.83	13.88
$\text{SiO}_2/\text{WO}_3(50/50)$	290	0.4502	3.19	68.08
$\text{SiO}_2/\text{WO}_3(40/60)$	290	0.33663	3.85	56.50
$\text{SiO}_2/\text{WO}_3(30/70)$	294	0.01715	18.72	11.78
$\text{SiO}_2/\text{WO}_3(20/80)$	305	0.57659	2.68	85.49
$\text{SiO}_2/\text{WO}_3/\text{ZnO}(70/30)$	290	0.7093	2.25	96.69
$\text{SiO}_2/\text{WO}_3/\text{ZnO}(80/20)$	287	0.76122	2.10	102.49
$\text{SiO}_2/\text{WO}_3/\text{ZnO}(90/10)$	290	0.58877	2.63	82.61

### 3.5 UV-Vis spectroscopy

As shown in Fig. 7, the  $\text{SiO}_2/\text{WO}_3(80/20)$  film sample exhibited absorption in the UVA light region (315–400 nm). When the  $\text{WO}_3$  content of the film sample increased, the absorption band widened to the visible light region and the optical absorption of the composite film samples in the UVA light region was significantly improved. Pure  $\text{WO}_3$  film exhibited absorption in both UV and visible light regions, while pure  $\text{SiO}_2$  film exhibited low absorption only in the UV range (~300 nm). As expected  $\text{WO}_3$  contribution improved the optical absorption ability of the composite film. It would be appropriate to extend the photocatalytic reaction application to the visible light region. But, it can be

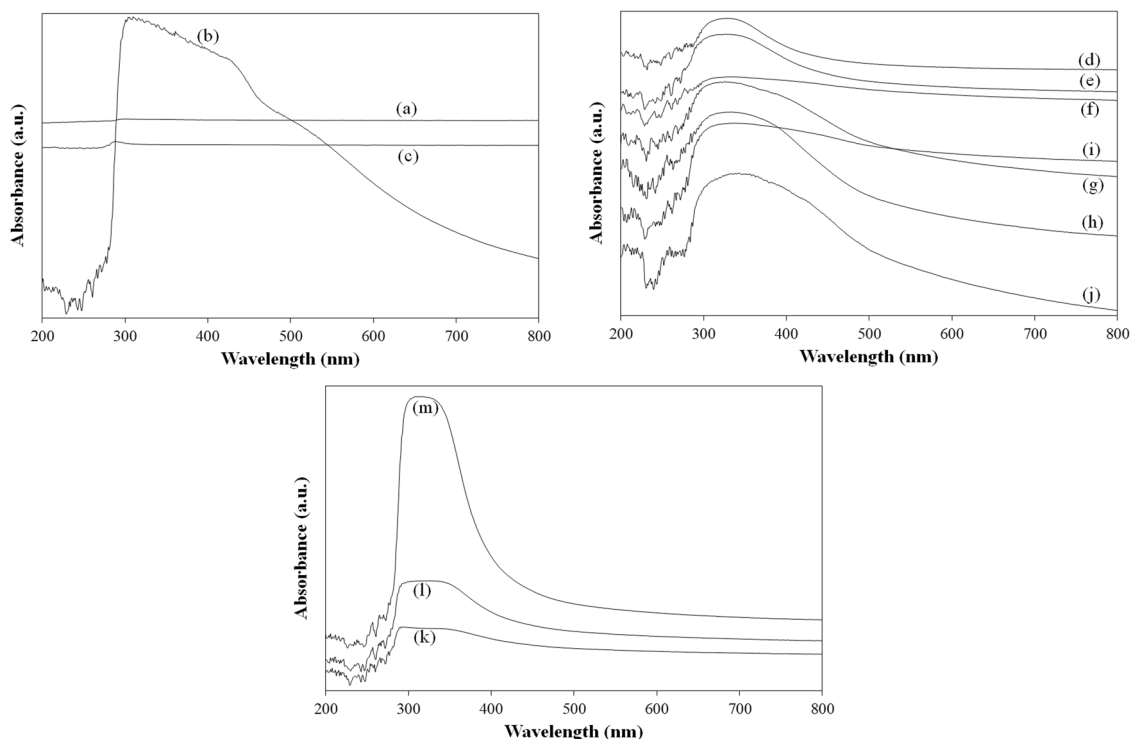


**Fig. 7** Absorbance spectrum of (a)  $\text{SiO}_2$ , (b)  $\text{WO}_3$ , (c)  $\text{ZnO}$ , (d)  $\text{SiO}_2/\text{WO}_3(80/20)$ , (e)  $\text{SiO}_2/\text{WO}_3(70/30)$ , (f)  $\text{SiO}_2/\text{WO}_3(60/40)$ , (g)  $\text{SiO}_2/\text{WO}_3(50/50)$ , (h)  $\text{SiO}_2/\text{WO}_3(40/60)$ , (i)  $\text{SiO}_2/\text{WO}_3(30/70)$ , (j)  $\text{SiO}_2/\text{WO}_3(20/80)$ , (k)  $\text{SiO}_2/\text{WO}_3/\text{ZnO}(90/10)$ , (l)  $\text{SiO}_2/\text{WO}_3/\text{ZnO}(80/20)$  and (m)  $\text{SiO}_2/\text{WO}_3/\text{ZnO}(70/30)$



detrimental to the solar cell in terms of the efficiency. The photovoltaic market is mainly based on crystalline silicon, which can absorb almost one-third of usable solar photons. Photons in the red and near-infrared portion of the sun light spectrum (700–1100 nm) can be absorbed by the silicon. Photons with shorter wavelengths can be absorbed by the silicon. But, they have more energy than the silicon needs, causing the excess energy to be released as heat [38]. As specified before  $\text{WO}_3$  widened the edge of the absorption band to the visible light, which might lead to a decrease in the intensity of the sun light reaching to the absorber layer of the solar cell. Any decrease in the number of photons in the visible light region (400–700 nm) might affect the solar cell efficiency.

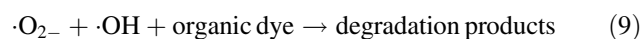
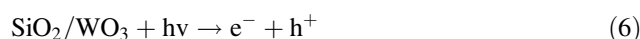
As estimated from the Tauc plot (Fig S2), the optical band gap energy of pure  $\text{SiO}_2$  and  $\text{WO}_3$  films were estimated to be 4.80 eV and 2.35 eV, respectively. According to Fig. S3, the optical band gap energy was calculated to be 2.95 eV, 2.80 eV, 2.15 eV, 2.35 eV, 2.45 eV, 2.00 eV and 2.25 eV for  $\text{SiO}_2/\text{WO}_3(80/20)$ ,  $\text{SiO}_2/\text{WO}_3(70/30)$ ,  $\text{SiO}_2/\text{WO}_3(60/40)$ ,  $\text{SiO}_2/\text{WO}_3(50/50)$ ,  $\text{SiO}_2/\text{WO}_3(40/60)$ ,  $\text{SiO}_2/\text{WO}_3(30/70)$  and  $\text{SiO}_2/\text{WO}_3(20/80)$ , respectively. It was expected that the optical band gap energy would decrease as the  $\text{WO}_3$  content of the composite film sample increased. The optical band gap energy of the composite film samples ranged from 2.00 eV to 2.95 eV.

The UV-Vis absorption spectrum of the  $\text{SiO}_2/\text{WO}_3/\text{ZnO}$  film samples is also shown in Fig. 7. The  $\text{SiO}_2/\text{WO}_3/\text{ZnO}(90/10)$  film sample has a weak absorption in the UV region (in the range of 250–400 nm). The intensity of the absorption band increased as the ZnO content of the film sample increased. Since the solar cell generates electricity by absorbing mostly the visible light region of the incoming sunlight, absorption in the UV light range was not expected to have a negative impact on the efficiency of the solar cell. According to the Tauc plot analysis (Fig. S4), the optical band gap energy was estimated to be 2.70 eV, 2.95 eV and 3.20 eV for the  $\text{SiO}_2/\text{WO}_3/\text{ZnO}(90/10)$ ,  $\text{SiO}_2/\text{WO}_3/\text{ZnO}(80/20)$  and  $\text{SiO}_2/\text{WO}_3/\text{ZnO}(70/30)$  film samples, respectively. The optical band gap of the  $\text{SiO}_2/\text{WO}_3/\text{ZnO}$  film sample was widened with an increase in the ZnO content, which might be detrimental to the photocatalytic activity and beneficial to the solar cell efficiency.

### 3.6 Photocatalytic dye degradation efficiency

$\text{WO}_3$  has been widely studied as a photocatalyst due to its superior properties such as photostability, non-toxicity, chemical and thermal stability. In addition, it exhibits excellent solar radiation absorption due to its favorable band gap [39]. However, there is a main problem, limiting the practical application of  $\text{WO}_3$ . The rapid recombination of the photoexcited electrons with holes leads to a low quantum

efficiency and photocatalytic dye degradation efficiency. In literature, many attempts have been performed to reduce the recombination rate of the photoinduced charge carriers on the photocatalysts. Coupling  $\text{WO}_3$  with another semiconductor can reduce the recombination rate of the mobile charge carriers [39, 40]. Within the scope of the coupling  $\text{WO}_3$  with another semiconductor,  $\text{WO}_3$  was combined with  $\text{SiO}_2$  in the composite film structure. The photocatalytic degradation of methylene blue might be composed of four steps. When the film sample was exposed to UV light, the valence band electrons were excited to the conduction band to form photoexcited electron-hole pairs (6). The photoinduced charge carriers transferred to the surface of the film sample and reacted with the dye molecules. The surface adsorbed  $\text{H}_2\text{O}$  molecules might be oxidized by the photogenerated holes to hydroxyl radicals (7) and the dissolved  $\text{O}_2$  molecules might be reduced by the photogenerated electrons to superoxide radicals on the surface of the film samples (8). Both of these radicals are highly active and can degrade any organic molecules into simple molecules like  $\text{H}_2\text{O}$  and  $\text{CO}_2$  (9) [41].



Figures S5 and S6 illustrate UV-Vis absorption spectra of methylene blue in the presence of pure and the  $\text{SiO}_2/\text{WO}_3$  composite film samples. The absorption intensity decreased gradually with time under the UVA light irradiation for all film samples. At the end of 240 min of UVA light irradiation, the maximum absorption peak of methylene blue decreased to the lowest value with the  $\text{SiO}_2/\text{WO}_3(30/70)$  sample, which means that the highest photocatalytic dye degradation was obtained with the specified film sample. The photocatalytic dye degradation efficiency of the as-prepared film samples was calculated using the initial absorbance of the dye solution and the absorbance value of methylene blue solution exposed to the UVA light irradiation. In order to better compare the photocatalytic activity of the  $\text{SiO}_2/\text{WO}_3$  composite films, all dye degradation efficiency values were plotted in Fig. 8. After 240 min of the UVA light irradiation, the photocatalytic dye degradation efficiency was 25.2, 46.1, 53.5, 68.8, 75.2, 84.6, and 58.2% for the  $\text{SiO}_2/\text{WO}_3(80/20)$ ,  $\text{SiO}_2/\text{WO}_3(70/30)$ ,  $\text{SiO}_2/\text{WO}_3(60/40)$ ,  $\text{SiO}_2/\text{WO}_3(50/50)$ ,  $\text{SiO}_2/\text{WO}_3(40/60)$ ,  $\text{SiO}_2/\text{WO}_3(30/70)$  and  $\text{SiO}_2/\text{WO}_3(20/80)$  films, respectively. The  $\text{SiO}_2/\text{WO}_3(30/70)$  film sample exhibited the highest photocatalytic activity. When compared with pure  $\text{SiO}_2$  and pure  $\text{WO}_3$  film samples, there was a significant enhancement in

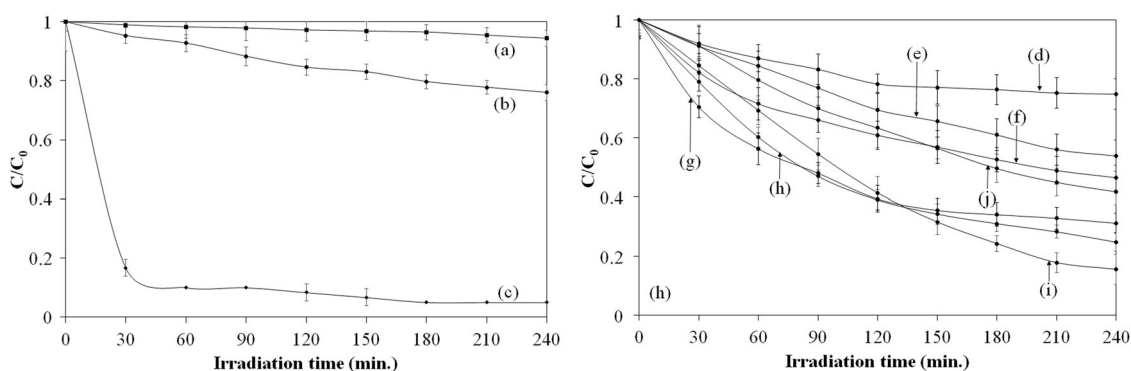


**Fig. 8** Photocatalytic degradation rate of methylene blue on (a) SiO<sub>2</sub>, (b) WO<sub>3</sub>, (c) ZnO, (d) SiO<sub>2</sub>/WO<sub>3</sub>(80/20), (e) SiO<sub>2</sub>/WO<sub>3</sub>(70/30), (f) SiO<sub>2</sub>/WO<sub>3</sub>(60/40), (g) SiO<sub>2</sub>/WO<sub>3</sub>(50/50), (h) SiO<sub>2</sub>/WO<sub>3</sub>(40/60), (i) SiO<sub>2</sub>/WO<sub>3</sub>(30/70), (j) SiO<sub>2</sub>/WO<sub>3</sub>(20/80) films

the photocatalytic activity of the composite film samples (Fig. 8). Pure SiO<sub>2</sub> and pure WO<sub>3</sub> film samples were able to degrade 5.6 and 24.0% of methylene blue, respectively, after 240 min of the UVA light irradiation. According to Hu and his coworkers (2012), the interaction between SiO<sub>2</sub> and WO<sub>3</sub> in the composite structure might lead to the formation of the oxygen vacancy. The oxygen vacancy led to the formation of a defect state between the conduction and valence bands of WO<sub>3</sub>. The specified defect state might act as the hole trap, suppressing the recombination rate of the photogenerated electron-hole pairs [42]. Any effect that decreases the recombination rate of the photoinduced electron-hole pairs or increases the number of charge carriers positively affects the photocatalytic efficiency. In literature, according to Li and his coworkers (2014), the SiO<sub>2</sub> surface was rich in the hydroxyl radicals in the aqueous medium. The increase in the number of the hydroxyl radicals on the SiO<sub>2</sub> surface improved the ability of the composite sample to retain the adsorbed water, which might result in an increase in the reaction rate between the dye molecules and WO<sub>3</sub>. In addition, SiO<sub>2</sub> had a high tendency to trap the photoexcited electrons in its conduction band, suppressing the recombination rate of the photogenerated electron-hole pairs [17]. The electron trapping ability of SiO<sub>2</sub> might also be the reason for the significant enhancement in the photoactivity of the SiO<sub>2</sub>/WO<sub>3</sub> composite film sample. The trapping of the photoexcited electrons of WO<sub>3</sub> on the conduction band of SiO<sub>2</sub> might contribute to the effective separation of the mobile charge carrier, which are necessary to form the active radicals responsible for the degradation of the organic dye molecules. The weight ratio of SiO<sub>2</sub> to WO<sub>3</sub> was critical in terms of the photocatalytic activity. The weight ratio of the composite constituents might affect the contact effectiveness between SiO<sub>2</sub> and WO<sub>3</sub> particles. The excess of any of the composite components might reduce the contact between the SiO<sub>2</sub> and WO<sub>3</sub> particles. According to Fig. 8, the optimum composition (SiO<sub>2</sub>/WO<sub>3</sub>(30/70)) might provide the effective

contact between SiO<sub>2</sub> and WO<sub>3</sub> particles. Increasing or decreasing the WO<sub>3</sub> content of the composite from the optimum value might reduce the contact interface between SiO<sub>2</sub> and WO<sub>3</sub> particles, suppressing the effective transfer of the photoinduced electron-hole pairs between the composite constituents. Hence, many photoinduced charge carriers might recombine on SiO<sub>2</sub> and WO<sub>3</sub>, decreasing the photocatalytic dye degradation efficiency [43]. To study the effect of the light source on the photocatalytic activity of the film, the optimum composition (SiO<sub>2</sub>/WO<sub>3</sub>) was also tested under visible light irradiation. According to the photocatalytic dye degradation results, there was no significant difference in the dye degradation rates (Fig. S7). The SiO<sub>2</sub>/WO<sub>3</sub>(30/70) film exhibited 83.6% dye degradation rate under the visible light irradiation after 240 min. Hence, no significant effect of the light source on the photocatalytic activity was observed.

According to [43], the bottom energy state of the conduction band for WO<sub>3</sub> and SiO<sub>2</sub> were equivalent to  $-0.66$  eV and  $-0.56$  eV (vs NHE), respectively. The top energy state of the valence band for WO<sub>3</sub> and SiO<sub>2</sub> were equivalent to 2.26 eV and 3.65 eV (vs NHE), respectively. Coupling WO<sub>3</sub> and SiO<sub>2</sub> in the composite structure affected the charge transfer by different pathways, leading to an improvement in the photocatalytic activity [43]. The contact points between SiO<sub>2</sub> and WO<sub>3</sub> might have a significant role in suppressing the recombination of the photoexcited electron-hole pairs, which was also confirmed by [43]. The SiO<sub>2</sub>/WO<sub>3</sub> composite could form hydroxyl radicals from surface adsorbed water molecules because the composite could provide sufficient driving force for the formation of the oxidation reaction of OH/•OH (1.99 eV vs. NHE). In addition, the composite sample could form superoxide radicals from surface adsorbed oxygen molecules because the conduction band position of both WO<sub>3</sub> and SiO<sub>2</sub> could overcome the thermodynamic barrier of the reduction reaction of O<sub>2</sub>/•O<sub>2</sub><sup>-</sup> ( $-0.33$  eV vs NHE) [43]. Because of the potential differences in the band energy levels of SiO<sub>2</sub> and

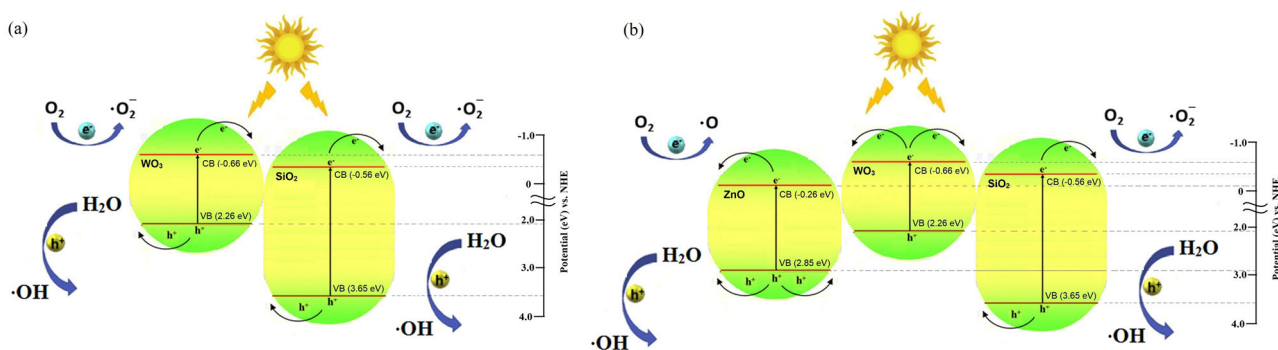


**Fig. 9** Proposed photocatalytic degradation mechanism of methylene blue on (a) SiO<sub>2</sub>/WO<sub>3</sub> film and (b) SiO<sub>2</sub>/WO<sub>3</sub>/ZnO film

**Table 3** Reaction rate constant values adjusted according to the pseudo-first-order kinetic model

Sample	k (min <sup>-1</sup> )	R <sup>2</sup>
SiO <sub>2</sub> /WO <sub>3</sub> (80/20)	0.0015	0.7897
SiO <sub>2</sub> /WO <sub>3</sub> (70/30)	0.0027	0.9913
SiO <sub>2</sub> /WO <sub>3</sub> (60/40)	0.0036	0.9088
SiO <sub>2</sub> /WO <sub>3</sub> (50/50)	0.0059	0.7879
SiO <sub>2</sub> /WO <sub>3</sub> (40/60)	0.0065	0.9369
SiO <sub>2</sub> /WO <sub>3</sub> (30/70)	0.0078	0.9905
SiO <sub>2</sub> /WO <sub>3</sub> (20/80)	0.0038	0.9970
Pure SiO <sub>2</sub>	0.0002	0.9705
Pure WO <sub>3</sub>	0.0012	0.9833
Pure ZnO	0.0163	0.2326
SiO <sub>2</sub> /WO <sub>3</sub> /ZnO(70/30)	0.0110	0.9705
SiO <sub>2</sub> /WO <sub>3</sub> /ZnO(80/20)	0.0088	0.9939
SiO <sub>2</sub> /WO <sub>3</sub> /ZnO(90/10)	0.0088	0.9914

WO<sub>3</sub>, the photoexcited electrons of WO<sub>3</sub> could transfer to the conduction band of SiO<sub>2</sub> (Fig. 9). The opposite was true for the photoexcited holes formed on SiO<sub>2</sub>. The photo-generated holes of SiO<sub>2</sub> could transfer to the valence band of WO<sub>3</sub>. Thus, the photoinduced electron-hole pairs might be effectively separated. The superoxide radicals might be generated directly or indirectly by the photoinduced electrons of SiO<sub>2</sub> and WO<sub>3</sub>. Similarly, the hydroxyl radicals might be formed directly or indirectly by the photoinduced holes of WO<sub>3</sub> and SiO<sub>2</sub> [43].

The Langmuir-Hinshelwood model was utilized to analyze the reaction rate of heterogeneous photocatalysis for the degradation of methylene blue on the film samples. The Langmuir-Hinshelwood model formula is given below [44]:

$$\ln(C_0/C) = kt \quad (10)$$

where C<sub>0</sub> and C are the concentration of methylene blue solution before and after the UVA light irradiation, respectively. In addition, k is the apparent pseudo-first-order reaction rate constant, which was obtained from the

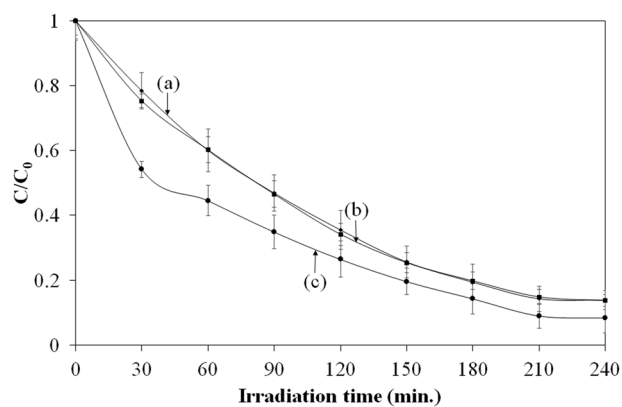


**Fig. 10** Photocatalytic degradation rate of methylene blue on (a) SiO<sub>2</sub>/WO<sub>3</sub>/ZnO(90/10), (b) SiO<sub>2</sub>/WO<sub>3</sub>/ZnO(80/20) and (c) SiO<sub>2</sub>/WO<sub>3</sub>/ZnO(70/30) films

plot of  $\ln(C/C_0)$  vs.  $t$  (Fig. S8). Fig. S8 confirmed that the pseudo-first-order was followed by the photocatalytic dye degradation reactions in the presence of the SiO<sub>2</sub>/WO<sub>3</sub> film samples. The reaction rate constant values were compared on Table 3. The highest reaction rate constant was obtained with the SiO<sub>2</sub>/WO<sub>3</sub>(30/70) film sample. Compared to pure SiO<sub>2</sub> and WO<sub>3</sub> film samples, a significant increase in the reaction rate of the photocatalytic degradation of methylene blue was obtained with the SiO<sub>2</sub>/WO<sub>3</sub>(30/70) film sample (Table 3).

To enhance the photocatalytic dye degradation efficiency of the SiO<sub>2</sub>/WO<sub>3</sub> composite system, it was also coupled with a well-known photocatalyst ZnO. Since the highest photocatalytic activity was obtained with the SiO<sub>2</sub>/WO<sub>3</sub>(30/70) film sample, this composition was utilized to prepare the SiO<sub>2</sub>/WO<sub>3</sub>/ZnO composite films. Fig. S9 shows the absorption spectrum of methylene blue in the presence of SiO<sub>2</sub>/WO<sub>3</sub>/ZnO film samples. A decrease in the absorption spectrum intensity was observed with time under the UVA light irradiation. Figure 10 illustrates the percentage of the photocatalytic degradation of the model dye in the aqueous solution using the SiO<sub>2</sub>/WO<sub>3</sub>/ZnO film samples. Compared to the optimum SiO<sub>2</sub>/WO<sub>3</sub> composite film sample (SiO<sub>2</sub>/

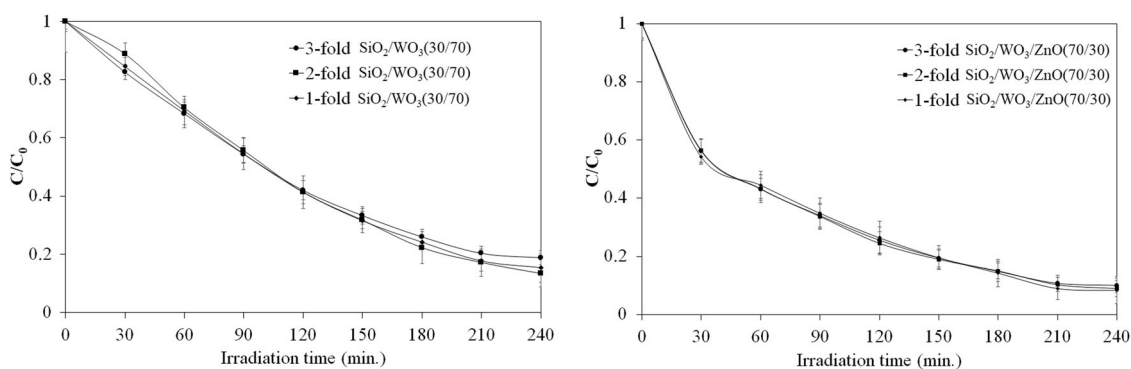


**Fig. 11** Photocatalytic degradation rate of the model dye on  $\text{SiO}_2/\text{WO}_3(30/70)$  film and  $\text{SiO}_2/\text{WO}_3/\text{ZnO}(70/30)$  film prepared by varying dip-coating cycles

$\text{WO}_3(30/70)$ ), the photocatalytic degradation percentage of methylene blue was enhanced on the  $\text{SiO}_2/\text{WO}_3/\text{ZnO}$  film sample. Combining the optimum  $\text{SiO}_2/\text{WO}_3$  composition with ZnO seemed to be effective in terms of the photocatalytic activity. The maximum dye degradation percentage for  $\text{SiO}_2/\text{WO}_3/\text{ZnO}(90/10)$ ,  $\text{SiO}_2/\text{WO}_3/\text{ZnO}(80/20)$  and  $\text{SiO}_2/\text{WO}_3/\text{ZnO}(70/30)$  was obtained as 86.1, 86.3 and 91.6%, respectively (Fig. 10).

Figure S10 illustrates the kinetics of the photocatalytic degradation of the model dye. The degradation kinetics seemed to fit to the pseudo-first-order reaction model (Table 3). The reaction rate constant value for  $\text{SiO}_2/\text{WO}_3/\text{ZnO}(90/10)$ ,  $\text{SiO}_2/\text{WO}_3/\text{ZnO}(80/20)$  and  $\text{SiO}_2/\text{WO}_3/\text{ZnO}(70/30)$  were 0.0088, 0.0088 and 0.0110  $\text{min}^{-1}$ , respectively. The reaction rate constant values revealed that the  $\text{SiO}_2/\text{WO}_3/\text{ZnO}$  composites were more active to degrade the dye molecules under the UVA irradiation. With the contribution of ZnO to the  $\text{SiO}_2/\text{WO}_3$  composite system, the reaction rate was increased by about 1.4 times. Due to its high photocatalytic activity, ZnO might enhance the photocatalytic dye degradation efficiency of the resulting composite system.

According to Lu and his coworkers (2016), the bottom energy state of the conduction band for ZnO was equivalent to  $-0.26$  eV (vs NHE) and the top energy state of the valence band for ZnO was equivalent to 2.85 eV (vs NHE) [45]. When ZnO was combined with  $\text{SiO}_2/\text{WO}_3$ , the conduction band potential of ZnO was more positive than that of  $\text{SiO}_2$  and  $\text{WO}_3$  (Fig. 9). In addition, the valence band potential of ZnO was more positive than that of  $\text{WO}_3$ . Thus, the photoinduced electrons of both  $\text{WO}_3$  and  $\text{SiO}_2$  might transfer to the conduction band of ZnO. Also, the photoinduced holes of ZnO might transfer to the valence band of  $\text{WO}_3$ . Hence, the  $\text{SiO}_2/\text{WO}_3/\text{ZnO}$  heterostructure might effectively separate the photogenerated mobile charge carriers on the  $\text{SiO}_2/\text{WO}_3$  composite, further improving the photocatalytic dye degradation efficiency. The effectively separated electron-hole pairs could migrate to the photocatalyst surface to form the active radicals necessary to

degrade the methylene blue molecules. ZnO in the composite structure could also form the hydroxyl radical from the surface adsorbed water molecules because the redox potential of the couple  $\text{OH}^\cdot/\text{OH}$ , which is 1.99 eV vs. NHE, was more negative than the valence band edge potential of ZnO. According to the redox potentials of the couple  $\text{O}_2/\text{O}_2^\cdot-$  ( $-0.33$  eV vs. NHE), the surface adsorbed  $\text{O}_2$  molecules could not be reduced by the photogenerated electrons of ZnO to superoxide anion radicals ( $\text{O}_2^\cdot-$ ) [43].

Within the scope of the optimization study, the effect of the number of the dip-coating cycle on the photocatalytic activity was also studied. According Fig. 11,  $\text{SiO}_2/\text{WO}_3(30/70)$  (1-fold coating),  $\text{SiO}_2/\text{WO}_3(30/70)$  (2-fold coating),  $\text{SiO}_2/\text{WO}_3(30/70)$  (3-fold coating) film samples exhibited the dye degradation efficiency of 84.6, 86.6 and 81.1%, respectively, after 240 min. Figure 11 also illustrates the photocatalytic degradation of the model dye on  $\text{SiO}_2/\text{WO}_3/\text{ZnO}(70/30)$  (1-fold coating),  $\text{SiO}_2/\text{WO}_3/\text{ZnO}(70/30)$  (2-fold coating) and  $\text{SiO}_2/\text{WO}_3/\text{ZnO}(70/30)$  (3-fold coating) film samples, respectively. When the model dye was irradiated on the 1-fold coated  $\text{SiO}_2/\text{WO}_3/\text{ZnO}(70/30)$ , 2-fold coated  $\text{SiO}_2/\text{WO}_3/\text{ZnO}(70/30)$  and 3-fold coated  $\text{SiO}_2/\text{WO}_3/\text{ZnO}(70/30)$  films samples, the degradation of methylene blue reached the maximum of 91.6, 91.0 and 90.0%, respectively, after 240 min of the UVA light irradiation. It was observed that the degradation of the model dye was weakly dependent on the number of the dip-coating cycle.

### 3.7 Solar cell efficiency

Glass slides coated with the  $\text{SiO}_2/\text{WO}_3$  or  $\text{SiO}_2/\text{WO}_3/\text{ZnO}$  film samples were used to measure the effect of the coated film on the real solar cell. Figure 12 illustrates the variation of the obtained voltage with the current by an uncoated and coated solar cells. The fill factor (FF) and the efficiency of the uncoated (standard) solar cell and coated solar cells were summarized on Table 4. In general, relatively higher solar cell efficiency was achieved with the composite films including high  $\text{SiO}_2$  content. The solar cell efficiency



**Table 4** Efficiency of the uncoated (standard) and coated solar cells

Sample	$V_m$ (V)	$I_m$ (A)	$V_{oc}$	$I_{sc}$	F.F	A (m <sup>2</sup> )	$P_{out}$ (W/m <sup>2</sup> )	$P_{in}$ (W/m <sup>2</sup> )	$\eta$ (%)
Standard	0.30	0.147	0.475	0.224	0.415	0.0008	55.13	1000	5.51
SiO <sub>2</sub>	0.315	0.144	0.473	0.217	0.442	0.0008	56.70	1000	5.67
ZnO	0.315	0.132	0.471	0.204	0.433	0.0008	51.98	1000	5.20
WO <sub>3</sub>	0.207	0.104	0.299	0.152	0.474	0.0008	26.91	1000	2.69
SiO <sub>2</sub> /WO <sub>3</sub> (80/20)	0.289	0.150	0.434	0.227	0.440	0.0008	54.19	1000	5.42
SiO <sub>2</sub> /WO <sub>3</sub> (70/30)	0.306	0.147	0.442	0.214	0.476	0.0008	56.23	1000	5.62
SiO <sub>2</sub> /WO <sub>3</sub> (60/40)	0.307	0.140	0.461	0.211	0.442	0.0008	53.73	1000	5.37
SiO <sub>2</sub> /WO <sub>3</sub> (50/50)	0.292	0.161	0.421	0.235	0.475	0.0008	58.77	1000	5.88
SiO <sub>2</sub> /WO <sub>3</sub> (40/60)	0.261	0.128	0.413	0.195	0.415	0.0008	41.76	1000	4.18
SiO <sub>2</sub> /WO <sub>3</sub> (30/70)	0.266	0.119	0.385	0.175	0.469	0.0008	39.57	1000	3.96
SiO <sub>2</sub> /WO <sub>3</sub> (20/80)	0.264	0.129	0.419	0.197	0.413	0.0008	42.57	1000	4.26
SiO <sub>2</sub> /WO <sub>3</sub> /ZnO(90/10)	0.302	0.145	0.454	0.218	0.442	0.0008	54.74	1000	5.47
SiO <sub>2</sub> /WO <sub>3</sub> /ZnO(80/20)	0.309	0.142	0.437	0.207	0.485	0.0008	54.85	1000	5.48
SiO <sub>2</sub> /WO <sub>3</sub> /ZnO(70/30)	0.290	0.142	0.459	0.217	0.413	0.0008	51.48	1000	5.15

experiment was performed under a solar light simulator. Due to its wide optical band gap, the SiO<sub>2</sub> film could transmit most of the incident light to the absorber layer of the solar cell. The WO<sub>3</sub> film coating, which has a narrower optical band gap than that of SiO<sub>2</sub>, could reduce the efficiency of the solar cell by absorbing more of the incoming light. The light transmittance spectroscopy supported this idea. The composite film samples with high SiO<sub>2</sub> content exhibited high transmittance in both UV and visible light regions. Compared to the uncoated solar cell (standard), higher efficiency was achieved by the solar cell including the SiO<sub>2</sub>/WO<sub>3</sub>(70/30) and SiO<sub>2</sub>/WO<sub>3</sub>(50/50) film samples, respectively. The reason for the improvement in the solar cell efficiency might be the reflective feature of the specified film coatings. Figure 12 also illustrates the voltage-current characteristics of the solar cell coated with the SiO<sub>2</sub>/WO<sub>3</sub>/ZnO film samples. To prepare the SiO<sub>2</sub>/WO<sub>3</sub>/ZnO film samples, the SiO<sub>2</sub>/WO<sub>3</sub>(30/70) film sample was utilized and coupled with ZnO in varying compositions. Compared to the SiO<sub>2</sub>/WO<sub>3</sub>(30/70) film coating, the solar cell efficiency slightly increased. The wide optical band gap and the anti-reflective feature of ZnO might be the possible reason for the improvement in the solar cell efficiency. When compared with the uncoated solar cell (standard), approximately the same efficiency value was obtained with the solar cell coated with the SiO<sub>2</sub>/WO<sub>3</sub>/ZnO(90/10) and SiO<sub>2</sub>/WO<sub>3</sub>/ZnO(80/20) films, respectively. As the ZnO content of the SiO<sub>2</sub>-WO<sub>3</sub>/ZnO films increased, the solar cell efficiency slightly decreased. To analyze the individual effect of the composite phases on the solar cell efficiency, the voltage-current characteristics of the solar cell coated with pure SiO<sub>2</sub>, pure WO<sub>3</sub> and pure ZnO films were also analyzed and their results were shown in Fig. 12. When compared with the standard solar cell, slightly higher and slightly lower efficiencies were achieved by the solar cell coated with pure SiO<sub>2</sub> film and pure ZnO film, respectively. On the other hand,

pure WO<sub>3</sub> film significantly reduced the efficiency of the standard cell (from 5.51 to 2.69).

Fill factor (FF) is one of the important parameters to determine the efficiency of a solar system. To get the maximum possible efficiency from a solar module, FF should be maximum and its value should approach one [46]. The fill factor, the ratio of the theoretical power to the maximum power, can be calculated by using the following relation (11):

$$FF = V_{MP}I_{MP}/V_{OC}I_{SC} \quad (11)$$

where  $V_{OC}$  is the open circuit voltage,  $I_{SC}$  is the short circuit current,  $V_{MP}$  is the voltage value at the maximum power point and  $I_{MP}$  is the current at the maximum power point [46]. The fill factor is known as a measure of the quality of a solar cell. Among the solar cells coated with the SiO<sub>2</sub>/WO<sub>3</sub> films, only the solar cell coated with the SiO<sub>2</sub>/WO<sub>3</sub>(20/80) film had a slightly lower FF value than the standard solar cell. Among the solar cells coated with the SiO<sub>2</sub>/WO<sub>3</sub>/ZnO films, only the solar cell coated with the SiO<sub>2</sub>/WO<sub>3</sub>/ZnO(70/30) film exhibited a slightly lower FF value compared to the standard solar cell (Table 4). The calculated FF values showed that the prepared film samples could be applied to the cover glass of the real photovoltaic system. In literature, only a few studies investigated possible effects of the film coating on the solar cell efficiency. Appasamy and his coworkers (2020) coated TiO<sub>2</sub>/carbon nanotube composite films on the cover glass of a solar cell. Both the coated and uncoated solar cells exhibited almost the similar voltage reading, indicating that the film coating did not deteriorate solar cell performance. The photocatalytic dye degradation efficiency of the composite film was about 72% after 420 min of UV light irradiation [47]. On the other hand, Soklic and his coworkers (2015) deposited TiO<sub>2</sub>/SiO<sub>2</sub> composite films on the cover glass of a solar cell. The solar cell efficiency decreased from 12.50 to 12.45% with

**Table 5** Effect of the number of the dip-coating cycle on the efficiency of the solar cell coated with SiO<sub>2</sub>/WO<sub>3</sub>(30/70) and SiO<sub>2</sub>/WO<sub>3</sub>/ZnO(70/30) films

Sample	V <sub>MP</sub> (V)	I <sub>MP</sub> (A)	V <sub>oc</sub>	I <sub>sc</sub>	F.F	A (m <sup>2</sup> )	P <sub>out</sub> (W/m <sup>2</sup> )	P <sub>in</sub> (W/m <sup>2</sup> )	η (%)
Standard	0.30	0.147	0.475	0.224	0.415	0.0008	55.13	1000	5.51
SiO <sub>2</sub> /WO <sub>3</sub> (30/70) 1-fold	0.266	0.119	0.385	0.175	0.469	0.0008	39.57	1000	3.96
SiO <sub>2</sub> /WO <sub>3</sub> (30/70) 2-fold	0.246	0.108	0.370	0.167	0.429	0.0008	33.21	1000	3.32
SiO <sub>2</sub> /WO <sub>3</sub> (30/70) 3-fold	0.198	0.097	0.316	0.148	0.411	0.0008	24.01	1000	2.04
SiO <sub>2</sub> /WO <sub>3</sub> /ZnO(70/30) 1-fold	0.290	0.142	0.459	0.217	0.413	0.0008	51.48	1000	5.15
SiO <sub>2</sub> /WO <sub>3</sub> /ZnO(70/30) 2-fold	0.262	0.119	0.393	0.180	0.441	0.0008	38.97	1000	3.90
SiO <sub>2</sub> /WO <sub>3</sub> /ZnO(70/30) 3-fold	0.250	0.124	0.361	0.180	0.477	0.0008	38.75	1000	3.88

the film coating. The photocatalytic dye degradation efficiency of the film coating was not investigated [10]. Compared to both studies, there was no similar significant change in the solar cell efficiency. However, higher photocatalytic dye degradation efficiency was achieved with the film coatings prepared within the scope of this study.

Within the scope of the optimization study, the effect of the number of the dip coating cycle on the solar cell efficiency was also studied (Fig. S11). According to Table 5, as the number of the dip-coating cycle increased, the efficiency of the solar cell coated with SiO<sub>2</sub>/WO<sub>3</sub> and SiO<sub>2</sub>/WO<sub>3</sub>/ZnO films slightly decreased. Maintaining or, if possible, increasing the efficiency of the solar cell is important for the applicability of the self-cleaning film layer on the solar cell. Therefore, increasing the number of the dip-coating cycle was useless in terms of the efficiency of the solar cell.

### 3.8 Water contact angle measurements

One of the most conventional techniques to investigate the photocatalytic self-cleaning feature of the film samples is the dye technique [2]. In the dye technique, the model dye is considered as contamination on the film and the photocatalytic degradation of the dye molecules under the UV light radiation is studied to reveal the self-cleaning feature of the film coatings [2]. According to the photocatalytic dye degradation experiments, the prepared film samples could degrade the model dye adsorbed on itself under the UVA light irradiation. Hence, methylene blue as the model dye could be decomposed to water and carbon dioxide. The photocatalytic degradation rate of the methylene blue could be measured by analyzing the rate of water formation through the contact angle measurement [2]. The formation of water molecules on the film surface could change the surface energy, leading to a reduction in the water contact angle. The photocatalytic activity of the film samples was also studied using the dye technique. The water contact angle measurement was performed on the film samples adsorbed by the methylene blue and exposed the UVA light irradiation.

Figure 13 illustrate the change of the water contact angle with the irradiation time, and Figs. S12 and S13 illustrate the images of the water droplets on the film samples. According to Fig. 13, the water contact angle exhibited a decrease with the irradiation time. The water contact angle of the SiO<sub>2</sub>/WO<sub>3</sub>(30/70) film and the SiO<sub>2</sub>/WO<sub>3</sub>/ZnO(70/30) film decreased from 45.1°, 64.1° to 29.2°, 45.4°, respectively, after 240 min of the UVA light irradiation. The water contact angle measurement revealed that the composite film samples were able to degrade the model dye adsorbed on itself with time and the film samples exhibited photocatalytic activity. Both the photocatalytic dye degradation and the water contact angle measurements verified the high photocatalytic activity of the SiO<sub>2</sub>/WO<sub>3</sub>(30/70) and SiO<sub>2</sub>/WO<sub>3</sub>/ZnO(70/30) films. The hierarchical surface structure can increase the hydrophobicity of the surface. When a water droplet comes into contact with the film surface, because of the presence of a surface roughness on the film surface, a three-phase interface can be formed. The raised microstructure on the film surface directly contacts the water droplet, while a portion of the concave areas on the film surface, including an air cushion, prevents the water droplet from directly wetting the film surface, resulting in an increase in the water contact angle value [48]. Comparing both film samples (SiO<sub>2</sub>/WO<sub>3</sub>(30/70) and SiO<sub>2</sub>/WO<sub>3</sub>/ZnO(70/30)), the SiO<sub>2</sub>/WO<sub>3</sub>/ZnO(70/30) film exhibited higher water contact angle value. The reason for the increase in the water contact angle value might be due to an increase in the surface roughness with ZnO. A similar result was obtained by Khorshidi and his coworkers (2021). By introducing ZnO nanoparticles to an acrylic coating, there was an increase in the water contact angle from 88.3° to 90.2°. It was determined that the increase in the water contact angle was due to the increase in the surface roughness [2].

## 4 Conclusion

The objective of this study was to coat the top layer of the solar cell with composite (SiO<sub>2</sub>/WO<sub>3</sub> and SiO<sub>2</sub>/WO<sub>3</sub>/ZnO) films, which had the ability of self-cleaning under the UVA

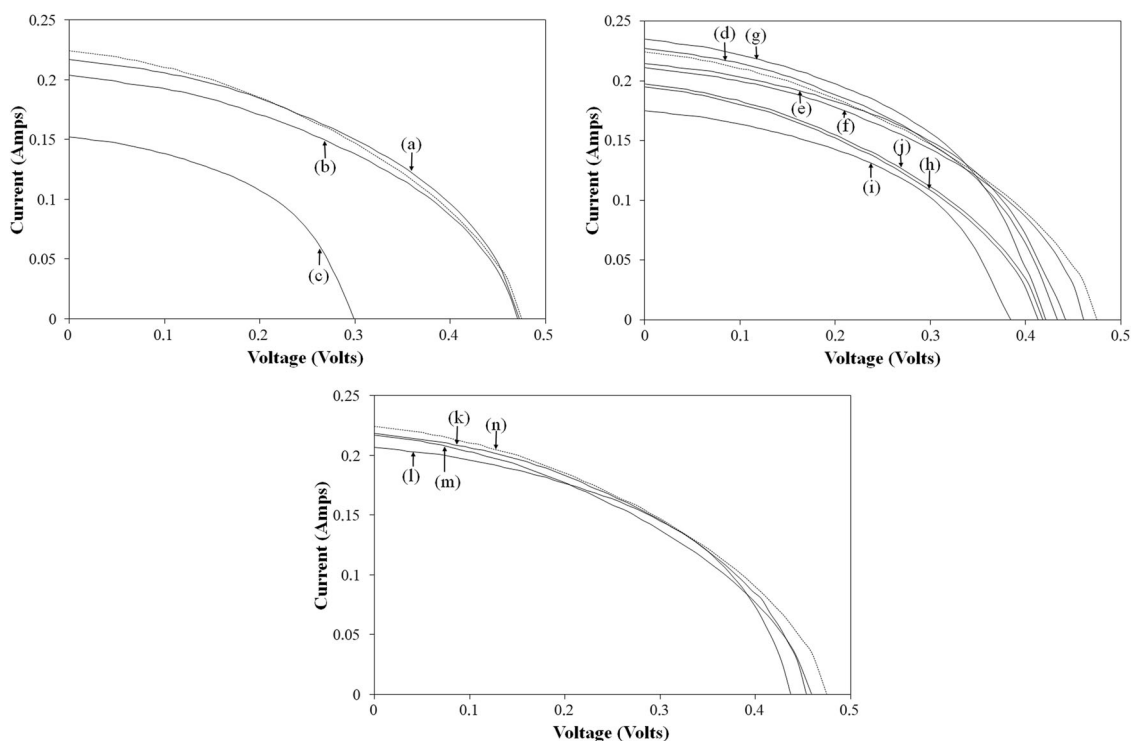


**Fig. 12** Current-voltage characteristics of solar cell coated with (a)  $\text{SiO}_2$ , (b)  $\text{WO}_3$ , (c)  $\text{ZnO}$ , (d)  $\text{SiO}_2/\text{WO}_3(80/20)$ , (e)  $\text{SiO}_2/\text{WO}_3(70/30)$ , (f)  $\text{SiO}_2/\text{WO}_3(60/40)$ , (g)  $\text{SiO}_2/\text{WO}_3(50/50)$ , (h)  $\text{SiO}_2/\text{WO}_3(40/60)$ , (i)

$\text{SiO}_2/\text{WO}_3(30/70)$ , (j)  $\text{SiO}_2/\text{WO}_3(20/80)$ , (k)  $\text{SiO}_2/\text{WO}_3/\text{ZnO}(90/10)$ , (l)  $\text{SiO}_2/\text{WO}_3/\text{ZnO}(80/20)$ , (m)  $\text{SiO}_2/\text{WO}_3/\text{ZnO}(70/30)$  films and including (n) uncoated glass slide

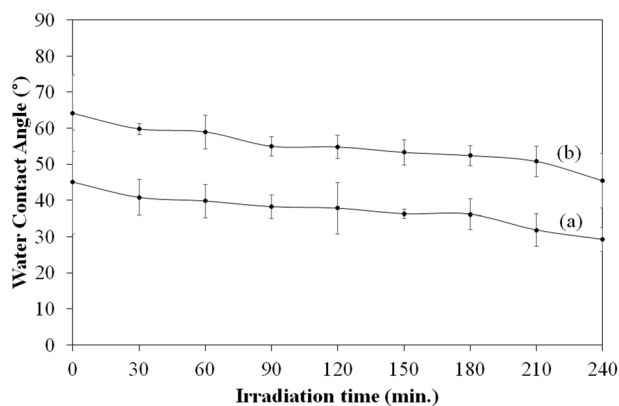


**Fig. 13** Variation in water contact angle with the irradiation time on (a)  $\text{SiO}_2/\text{WO}_3(30/70)$  and (b)  $\text{SiO}_2/\text{WO}_3/\text{ZnO}(70/30)$  films

light irradiation. The film coatings provided the self-cleaning process through the photocatalytic activity and the photoinduced hydrophilicity. Within this scope,  $\text{WO}_3$  was compounded with a highly transparent semiconductor  $\text{SiO}_2$ , minimizing the transmission loss on the solar cell.  $\text{ZnO}$  was also added into the film structure to provide an enhanced photocatalytic activity. The  $\text{SiO}_2/\text{WO}_3/\text{ZnO}$  film coatings exhibited high visible light transmittance and photocatalytic activity under the UVA light irradiation. The self-cleaning performance of the prepared film coatings was

also so high that the  $\text{SiO}_2/\text{WO}_3/\text{ZnO}$  film could degrade more than 90% of the model contaminant on itself within 240 min of the UVA light irradiation. The hydrophilicity of the  $\text{SiO}_2/\text{WO}_3$  and  $\text{SiO}_2/\text{WO}_3/\text{ZnO}$  film coated with the model contaminant increased with the irradiation, exhibiting the photocatalytic degradation efficiency of the prepared films. The current-voltage measurement of the solar cell coated with the  $\text{SiO}_2/\text{WO}_3/\text{ZnO}$  film did not exhibit any significant loss in efficiency. The results of the study revealed that the  $\text{SiO}_2/\text{WO}_3/\text{ZnO}$  film can be applied as a commercial product on the PV panel surfaces against the accumulation of any kinds of organic pollution, resulting in the reduction of the PV efficiency. Under the sun light, any kinds of organic contaminants deposited on the solar cell can be decomposed to small molecules like  $\text{H}_2\text{O}$  and  $\text{CO}_2$ . There is no need for rain to remove organic contaminants from the cover glass of the solar cell. On the other hand, the film coatings exhibited photoinduced hydrophilicity under the sun light. Thus, inorganic contaminants can also be easily removed from the cover glass of the solar cell in rainy weather. Although regular rain is required to remove inorganic contaminants, regular rain is not required to remove organic contaminants. As a conclusion, the film coatings, prepared within the scope this study, are more suitable to remove organic contaminants from the cover glass of the solar cell regardless of the rain event.

**Supplementary information** The online version contains supplementary material available at <https://doi.org/10.1007/s10971-024-06351-7>.

**Author contributions** All authors contributed to the study conception and design. Material preparation, data collection and analysis were performed by all authors.

**Funding** This research has been supported by The Scientific and Technological Research Council of Turkey (TÜBİTAK) and National Agency of Scientific Research and Innovation (NASRI) with the Project Number 122N383. Open access funding provided by The Scientific and Technological Research Council of Türkiye (TÜBİTAK).

## Compliance with ethical standards

**Conflict of interest** The authors declare no competing interests.

**Publisher's note** Springer Nature remains neutral with regard to jurisdictional claims in published maps and institutional affiliations.

**Open Access** This article is licensed under a Creative Commons Attribution 4.0 International License, which permits use, sharing, adaptation, distribution and reproduction in any medium or format, as long as you give appropriate credit to the original author(s) and the source, provide a link to the Creative Commons licence, and indicate if changes were made. The images or other third party material in this article are included in the article's Creative Commons licence, unless indicated otherwise in a credit line to the material. If material is not included in the article's Creative Commons licence and your intended use is not permitted by statutory regulation or exceeds the permitted use, you will need to obtain permission directly from the copyright holder. To view a copy of this licence, visit <http://creativecommons.org/licenses/by/4.0/>.

## References

- Estekhrayi SAZ, Amiri S (2017) Sol-gel preparation and characterization of antibacterial and self-cleaning hybrid nanocomposite coatings. *J Coat Technol Res* 14(6):1335–1343
- Khorshidi ZG, Jallab M, Moghbelli E, Goudarzi A, Ghaffari M (2021) Photocatalytic analysis of a hydrophilic acrylic coating/zinc oxide nanocomposite on glass substrate. *Polym-Plast Technol Mater* 60(11):1220–1232
- Pakdel E, Zhao H, Wang JF, Tang B, Varley RJ, Wang XG (2021) Superhydrophobic and photocatalytic self-cleaning cotton fabric using flower-like N-doped TiO<sub>2</sub>/PDMS coating. *Cellulose* 28(13):8807–8820
- Watte J, Van Zele M, De Buysser K, Van Driessche I (2018) Recent advances in low-temperature deposition methods of transparent, photocatalytic TiO<sub>2</sub> coatings on polymers. *Coatings* 8(4):131
- Gao Q, Wu XM, Cai LG (2021) Facial synthesis of K<sub>0.3</sub>WO<sub>3</sub>/Ag nanocomposites for self-cleaning energy efficient window coatings. *J Alloy Compd* 856:157069
- Luevano-Hipolito E, Torres-Martinez LM, Cantu-Castro LVF (2019) Self-cleaning coatings based on fly ash and bismuth-photocatalysts: Bi<sub>2</sub>O<sub>3</sub>, Bi<sub>2</sub>O<sub>2</sub>CO<sub>3</sub>, BiOI, BiVO<sub>4</sub>, BiPO<sub>4</sub>. *Constr Build Mater* 220:206–213
- Rudakova AV, Emeline AV (2021) Photoinduced hydrophilicity of surfaces of thin films. *Colloid J* 83(1):20–48
- Syafiq A, Pandey AK, Adzman NN, Abd Rahim N (2018) Advances in approaches and methods for self-cleaning of solar photovoltaic panels. *Sol Energy* 162:597–619
- Benöhr M, Gebremedhin A (2021) Photovoltaic systems for road networks. *Int J Innov Sci Technol* 4(2):672–684.
- Soklic A, Tasbihi M, Kete M, Stangar UL (2015) Deposition and possible influence of a self-cleaning thin TiO<sub>2</sub>/SiO<sub>2</sub> film on a photovoltaic module efficiency. *Catal Today* 252:54–60
- Aubell JP, Gebremedhin A (2021) Framed- or frameless photovoltaic in snow experiencing climates. *Int J Innov Sci Technol* 4(3):742–753.
- Thwala MM, Dlamini LN (2020) Photocatalytic reduction of Cr(VI) using Mg-doped WO<sub>3</sub> nanoparticles. *Environ Technol* 41(17):2277–2292
- Nagarjuna R, Challagulla S, Sahu P, Roy S, Ganesan R (2017) Polymerizable sol-gel synthesis of nano-crystalline WO<sub>3</sub> and its photocatalytic Cr(VI) reduction under visible light. *Adv Powder Technol* 28(12):3265–3273
- Ai L, Jia D, Guo N, Xu M, Zhang S, Wang L, Jia L (2020) Cl-doped Bi<sub>2</sub>S<sub>3</sub> homojunction nanorods with rich-defects for collaboratively boosting photocatalytic reduction performance. *Appl Surf Sci* 529:147002
- Zhou G, Long L, Wang P, Hu Y, Zhang Q, Liu C (2020) Designing CuO/ZnO nanoforest device toward optimal photocatalytic performance through structure and facet engineering. *Mater Lett* 273:127907
- Carvalho LM, Soares AF, Lima MS, Cruz-Filho JF, Dantas TCM, Luz GE (2021) 2,4-Dichlorophenoxyacetic acid (2,4-D) photo-degradation on WO<sub>3</sub>-TiO<sub>2</sub>-SBA-15 nanostructured composite. *Environ Sci Pollut Res* 28(7):7774–7785
- Li J, Du X, Yao L, Zhang Y (2014) Synthesis of SnS<sub>2</sub>/WO<sub>3</sub> nanocomposite with enhanced photocatalytic activity. *Mater Lett* 121:44–46
- Shi J, Liao R, Jia R, Liu Y, Wu D, Chang S, Zhang N, Gao G, Wang X, Hu D, Wu K (2023) A novel combustion drying synthesis route of 3D WO<sub>3</sub>-SiO<sub>2</sub> composite aerogels for enhanced adsorption and visible light photocatalytic activity. *J Non-Cryst Solids* 609:122259
- Zhang J, Guo Y, Xiong Y, Zhou D, Dong S (2017) An environmentally friendly Z-scheme WO<sub>3</sub>/CDots/CdS heterostructure with remarkable photocatalytic activity and anti-photocorrosion performance. *J Catal* 356:1–13
- Dozzi MV, Marzorati S, Longhi M, Coduri M, Artiglia L, Selli E (2016) Photocatalytic activity of TiO<sub>2</sub>-WO<sub>3</sub> mixed oxides in relation to electron transfer efficiency. *Appl Catal B-Environ* 186:157–165
- Ali AM, Ismail AA, Bouzid H, Harraz FA (2014) Sol-gel synthesis of ZnO-SiO<sub>2</sub> thin films: impact of ZnO contents on its photonic efficiency. *J Sol-Gel Sci Technol* 71:224–233
- Yao L, He JH (2014) Facile dip-coating approach to fabrication of mechanically robust hybrid thin films with high transmittance and durable superhydrophilicity. *J Mater Chem A* 2(19):6994–7003
- Li Y, Yang K, Xia B, Yang B, Yan L, He M, Yan H, Jiang B (2017) Preparation of mechanically stable triple-layer interference broadband antireflective coatings with self-cleaning property by sol-gel technique. *RSC Adv* 7:14660–14668
- Thilagavathi T, Venugopal D, Marnadu R, Chandrasekaran J, Alshahrani T, Shkir M (2021) An investigation on microstructural, morphological, optical, photoluminescence and photocatalytic activity of WO<sub>3</sub> for photocatalysis applications: an effect of annealing. *J Inorg Organomet Polym Mater* 31(3):1217–1230
- Wang M, Kim EJ, Chung JS, Shin EW, Hahn SH, Lee KE, Park C (2006) Influence of annealing temperature on the structural and optical properties of sol-gel prepared ZnO thin films. *Phys Status Solidi A-Appl Mat* 203:2418–2424
- Salvaggio MG, Passalacqua R, Stassi A (2016) Functional nano-textured titania-coatings with self-cleaning and antireflective properties for photovoltaic surfaces. *Sol Energy* 125:227–242



27. Ren YF, Li WT, Cao ZH, Jiao YP, Xu JJ, Liu P, Li S, Li X (2020) Robust TiO<sub>2</sub> nanorods-SiO<sub>2</sub> core-shell coating with high-performance self-cleaning properties under visible light. *Appl Surf Sci* 509:145377
28. Saravanan S, Dubey D, Raghvendra S (2020) Synthesis of SiO<sub>2</sub> nanoparticles by sol-gel method and their optical and structural properties. *Rom J Inf Sci Technol* 23:105–112
29. Gui-Long X, Changyun D, Yun L, Pi-Hui P, Jian H, Zhuoru Y (2011) Preparation and characterization of Raspberry-like SiO<sub>2</sub> particles by the sol-gel method. *Nanomater Nanotechnol* 1:21
30. Boran F, Çetinkaya S (2017) Synthesis, characterization and sensing behavior of WO<sub>3</sub> nanocrystalline powder for toluene vapor. *Acta Phys Pol A* 132(3):572–573
31. Aksoy S, Caglar Y (2019) Synthesis of Mn doped ZnO nanopowders by MW-HTS and its structural, morphological and optical characteristics. *J Alloy Compd* 781:929–935
32. Jayarambabu N, Kumari BS, Rao KV, Prabhu YT (2014) Germination and growth characteristics of mungbean seeds (*Vigna radiata* L.) affected by synthesized zinc oxide nanoparticles. *Int J Curr Eng Technol* 4(5):3411–3416
33. Sakthisabarimoorthi A, Dhas SMB, Jose M (2020) Study on optical nonlinearity of Au@ SiO<sub>2</sub> composite nanoparticles towards photonic applications. *Mater Chem Phys* 240:122154
34. Jerold Antony A, Mary Jelastin Kala S, Joel C, Biju Bennie R, Vivetha S (2022) Structural, optical, and magnetic properties of pristine and Cr doped WO<sub>3</sub> nanoparticles. *Inorg Nano-Met Chem* 52(7):951–960
35. Li X, He S, Liu X, Jin J, Meng H (2019) Polymer-assisted freeze-drying synthesis of Ag-doped ZnO nanoparticles with enhanced photocatalytic activity. *Ceram Int* 45(1):494–502
36. Muljani S, Wahyudi B, Sumada K (2016) Potassium silicate foliar fertilizer grade from geothermal sludge and pyrophyllite. In: *MATEC Web of Conferences* (Vol. 58, p. 01021). EDP Sciences
37. Ginley DS, Collins R, Cahen D (2012) In: *Ginley DS, Cahen D (eds) Fundamentals of Materials for Energy and Environmental Sustainability*, Cambridge University Press
38. Chahi M, Alcántara SP, Bouhekka A, Sib JD, Sanchez G, Chahed L (2020) The enhancement of near infrared light trapping in solar cells with backside crystalline silicon gratings: realization and characterization investigation. *Optik* 200:163142
39. Farhadian M, Sangpour P, Hosseinzadeh G (2015) Morphology dependent photocatalytic activity of WO<sub>3</sub> nanostructures. *J Energy Chem* 24(2):171–177
40. Wang SM, Yan XX, Deng DM, He HB, Lei YY, Shen X, Luo LQ (2019) Controllable synthesis and enhanced photocatalytic activity of B-TiO<sub>2</sub> nanospheres. *Micro Nano Lett* 14(7):740–743
41. Wu T, Li JY, Chang MQ, Song YH, Sun Q, Wang FK, Zou HF, Shi Z (2021) Photoluminescence properties and photocatalytic activities of SiO<sub>2</sub>@TiO<sub>2</sub>:Sm<sup>3+</sup> nanomaterials. *J Phys Chem* 149:109775
42. Hu SZ, Li FY, Fan ZP (2012) Preparation of SiO<sub>2</sub>-Coated TiO<sub>2</sub> Composite Materials with Enhanced Photocatalytic Activity Under UV Light. *Bull Korean Chem Soc* 33(6):1895–1899
43. Jourshabani M, Lee BK (2021) Unmasking the role of an amorphous/amorphous interface and a crystalline/amorphous interface in the transition of charge carriers on the CN/SiO<sub>2</sub>/WO<sub>3</sub> photocatalyst. *ACS Appl Mater Interfaces* 13(27):31785–31798
44. Hamed NKA, Ahmad MK, Hairom NHH, Faridah AB, Mamat MH, Mohamed A, Suriani AB, Soon CF, Fazli FIM, Mokhtar SM (2022) Photocatalytic degradation of methylene blue by flowerlike rutile-phase TiO<sub>2</sub> film grown via hydrothermal method. *J Sol-Gel Sci Technol* 102(3):637–648
45. Lu C, Zhimin BZ, Qin C, Dai L, Zhu A (2016) Facile fabrication of heterostructured cubic-CuFe<sub>2</sub>O<sub>4</sub>/ZnO nanofibers (c-CFZs) with enhanced visible-light photocatalytic activity and magnetic separation. *RSC Adv* 6:110155–110163
46. Sharma DK, Purohit G (2014) Analysis of the effect of fill factor on the efficiency of solar PV system for improved design of MPPT. In: 6th world conference on photo voltaic energy conversion
47. Appasamy JS, Kurnia JC, Assadi MK (2020) Synthesis and evaluation of nitrogen-doped titanium dioxide/single walled carbon nanotube-based hydrophilic self-cleaning coating layer for solar photovoltaic panel surface. *Sol Energy* 196:80–91
48. Liu G, Zhao T, Fei H, Li F, Guo W, Yao Z, Feng Z (2023) A review of various self-cleaning surfaces, durability and functional applications on building exteriors. *Constr Build Mater* 409:134084
49. Vulic T, Rudic O, Vucetic S, Lazar D, Ranogajec J (2015) Photocatalytic activity and stability of TiO<sub>2</sub>/ZnAl layered double hydroxide based coatings on mortar substrates. *Cem Concr Compos* 58:50–58
50. Noh HN, Myong SY (2014) Antireflective coating using a WO<sub>3</sub>-TiO<sub>2</sub> nanoparticle photocatalytic composition for high efficiency thin-film Si photovoltaic modules. *Sol Energy Mater Sol Cells* 121:108–113
51. Hosseini MS, Ebratkhahan M, Shayegan Z, Niaei A, Salari D, Rostami A, Raeisipour J (2020) Investigation of the effective operational parameters of self-cleaning glass surface coating to improve methylene blue removal efficiency; application in solar cells. *Sol Energy* 207:398–408
52. Jovanov V, Zecevic V, Vulic T, Ranogajec J, Fidanchevska E (2018) Preparation and characterization of protective self-cleaning TiO<sub>2</sub>/kaolin composite coating. *Mater Constr* 68(331):163